Synthesis, Characterization and Antibacterial Activity of Novel β-Cyclodextrin Polyurethane Materials

YueXing Chen
Lishui University
Jun Yan
North Minzu University
Yubin Zhang
Lishui University
Wenwen Chen
Lishui University
Zefeng Wang
Lishui University
Lingnan Wang (wangln07@163.com)
Wenzhou Institute, University of Chinese Academy of Sciences https://orcid.org/0000-0003-4783-6326

Original Research

Keywords: β-cyclodextrin, quaternary ammonium salt, multifunctional material, water purification

Posted Date: February 16th, 2021

DOI: https://doi.org/10.21203/rs.3.rs-200581/v1

Version of Record: A version of this preprint was published at Journal of Polymers and the Environment on August 7th, 2021. See the published version at https://doi.org/10.1007/s10924-021-02255-7.

Synthesis, Characterization and Antibacterial Activity of Novel β-cyclodextrin Polyurethane Materials

Yuexing Chen[1,a], Jun Yan[2,a], Yubin Zhang[1], Wenwen Chen[1], Zefeng Wang[1,*], Lingnan Wang[3,*]

[1]*College of Ecology, Lishui University, Lishui 323000, P. R. China.*

[2]*International Scientific and Technological Cooperation Base of Industrial Solid Waste Cyclic Utilization and Advanced Materials, North Minzu University, Yinchuan 750021, P. R. China*

[3]*Wenzhou Institute, University of Chinese Academy of Sciences, Wenzhou 325001, P. R. China*

[a]*These two authors contributed equally to this paper.*

**Correspondence should be addressed to Zefeng Wang (E-mail: shangk72@163.com) and Lingnan Wang (E-mail: wangln07@163.com)*

Abstract

The advanced water treatment taken by organic micro-pollution or microbiological pollution water resource has been a hot issue of public concern. In this article, a novel quaternary ammonium salt functionalized β-cyclodextrin polyurethane (QAS-β-CDPU) was successfully constructed for above-mentioned pollutants removal. By adjusting the proportion of the chlorine-containing monomers, we studied the effect of different quaternization degree (0%, 20%, 40%, 60%) on solvent resistance and thermal stability. Staphylococcus aureus are recognized as significant human bacterial pathogens, which were used as model bacteria to investigate the antibacterial activity by contact-killing tests. Methylene blue (MB) served as a toxic organic model to quantify the dye wastewater remediation efficiency. Research shows that the reaction of β-cyclodextrin and diisocyanate can form a cyclodextrin-based carbamate network structure. Since

both the cyclodextrin cavity and the carbamate network may remove the dye, the obtained polymer has a double advantage. Besides, the presence of quaternary ammonium groups enables QAS-β-CDPU to possess good bactericidal properties. When the quaternization degree is 60%, sterilization rate of QAS-β-CDPU comes to 97.3%. On basis of this simple, green and economical synthetic route, QAS-β-CDPU has the potential to become an ideal multifunctional material in water purification.

Keywords: β-cyclodextrin; quaternary ammonium salt; multifunctional material; water purification

1. Introduction

Water is the natural breeding ground for most pathogens. The levels of bacteria are treated as key indicators for water pollution. In countries like India, 80% of the diseases are caused by bacteria contamination in drinking water [1]. Water pollution with pathogenic bacteria pose a severe global threat to public health [2,3]. According to the 2017 World Health Organization (WHO) report, more than 25% of the global population lack access to safe water. Unclean water is more likely to contain a large variety of pathogens, such as Escherichia coli, Salmonella enteritidis, Vibrio cholerae and Shigella, which greatly increases the risk of waterborne diseases in humans [4]. Although the traditional disinfection methods are highly effective for microbial control in water treatment, for example, free chlorine, chloramine and ozone disinfection, it is easy to generate harmful disinfection by-products (DBPs), even numerous carcinogens [5]. In addition, the resistance of some pathogens, especially Cryptosporidium and Giardia, to conventional chemical disinfectants requires ever higher disinfectant dosage, which in turn exacerbates DBPs formation [6]. Therefore, the quest for novel water purifying materials without DBPs generation is of great significance.

Quaternary ammonium salt is deemed as a new type of cationic bactericide due to excellent cell membrane penetration, low toxicity, good environmental stability and superior biological activity [7]. Furthermore, it is inert to general redox agent and acids or bases, avoiding the formation of carcinogenic DBPs [8]. Unfortunately, the cationic

structure endows quaternary ammonium salt with high water solubility and uncontrollable diffusion, leading to short-lived dwell on the target surface and increased dose [9,10]. Contact active surfaces have drawn extensive attention for their non-release and long-term activity. In these surfaces, the antibacterial agents are covalently attached to polymer backbones to avoid releasing. Though this strategy it can not only achieves a long-term activity in an environmentally friendly way, but also avoid the drawback of rapid biocidal diffusion, obtaining satisfactory results in improving antibacterial efficiency and reducing residual toxicity [4]. Hence, modification to gain a long-acting slow-release antibacterial polymer is vital for widespread application of quaternary ammonium salt.

Recently, natural polymers like polysaccharides and their derivatives are considered as preferred low-cost adsorbents for wastewater treatment, attributing to their unique structure, physical and chemical properties, chemical stability, high reactivity, and good selectivity towards organics and metals [11]. Crini [12] reported a series of cheap polysaccharide-based dye adsorbents, one of the important polysaccharide derivatives is β-cyclodextrin (β-CD) [13]. β-CD is a kind of cyclic oligosaccharide produced from bacterial enzymatic hydrolysis of starch, featuring a hydrophilic exterior and a hydrophobic inner cavity [14]. The special structure can enable them to selectively combine various organic, inorganic and biological guest molecules into their cavities, and form stable host-guest inclusion complexes in their hydrophobic cavities [15]. Thus, β-CD may be favorable for removing pollutants in wastewater. However, the hydrophilic exterior makes β-CD readily dispersible in aqueous media, so it is difficult to adapt traditional separation methods to separate itself from the solution after the adsorption process, which may increase the costs considerably for industrial applications and/or cause secondary pollution [16]. In recent years, the emergence of cyclodextrin-based carbamate network structure from the reaction of cyclodextrin with diisocyanate link (hexamethylene diisocyanate (HMDI), toluene diisocyanate (TDI) or diphenylmethane diisocyanate (MDI)) provides an effective pathway to solve the above problems [17]. In fact, these bifunctional linkers help decrease the water solubility of cyclodextrin [17]. Moreover, since both the

cyclodextrin cavity and the carbamate network can remove the dye, the obtained polymer has a synergistic advantage [18].

Polyurethane (PU) is a most popular polymer material with excellent mechanical properties and good water resistance [18]. Polyurethane foam material has been widely applied in various fields as a carrier on account of its network structure, small bulk density, large surface area, and high adsorption efficiency [18]. Though there were lots of reports on quaternary ammonium salt-polyurethane-based antibacterial polymers [19] and cyclodextrin-polyurethane-based adsorption materials [20], quaternized cyclodextrin polyurethane has not yet been heard so far.

Herein, we take β-CD and diisocyanate as raw material to prepare cyclodextrin polyurethane matrix via internal emulsification. With help of quaternization reaction, it further synthesizes novel QAS-β-CDPU for removing bacteria and dyes from wastewater. Staphylococcus aureus, a microorganism related to human health, acts as model bacteria to evaluate antibacterial property of the polymer surface through contact-killing tests. MB, a toxic and carcinogenic cationic dye, behaves as a model dye to assess dye removal efficiency.

2. Experimental

2.1. Materials

β-CD, isophorone diisocyanate (IPDI), 2,2-dimethylolbutyric acid (DMBA), potassium persulfate (KPS), 2-hydroxyethyl methacrylate (HEMA), N, N-dimethylformamide (DMF), dibutyltin dilaurate (DY-12), triethylamine (TEA), ethanol (EA), 3-chloro-2-hydroxypropyl methacrylate (ClHPMA), trichloromethane, MB were purchased from Merck (Germany).

2.2. Preparation of QAS-β-CDPU

In brief, 4.0 g of β-CD was dissolved in 40 mL of DMF, followed by adding 6.66 g of IPDI, 0.6 g of hydrophilic chain-extender DMBA and 0.52 g of HEMA, then stirring constantly for 5 min. Afterward, 0.08 g of catalyst DY-12 was slowly added to

the dispersion and kept at 80°C for 3.5 h. After the reaction is completed, the resulting mixture was rapidly cooled down to 50°C. The pH of the solution was adjusted to neutral using 0.1 g of TEA and incubated for 5 min. 40 g of deionized water was poured into the cooled prepolymer under mechanical stirring to obtain vinyl-containing cyclodextrin-based polyurethane.

35g of the above yielded precipitate was treated with deionized water in a ratio of 1:1.2. Subsequently, 0.97g of the chlorine-containing vinyl monomer ClHPMA dispersed in 20 g of chloroform was injected by grafting method at one time, bubbling nitrogen through the mixture for 15-20 min, and then stirring at room temperature for 2 h. After confirming that the reaction system is uniformly agitated, the initiator KPS is added dropwise at 75°C and reacted for 24 h, the obtained product is denoted as Cl-β-CDPU. Finally, 0.75 g of triethylamine was added and stirred at ambient temperature for 24 h. The resultant sediment was rinsed repeatedly with ethanol and vacuum dried at 50°C for 24 h to gain pale yellow fine powder, which was recorded as QAS-β-CDPU-20%. As control experiments, by adjusting the mass ratio of the chlorine-containing monomers, the products with the quaternization degree of 0%, 40%, and 60% were obtained, which were named as QAS-β-CDPU-0%, QAS -β-CDPU-40% and QAS-β-CDPU-60%, respectively.

2.3. Preparation of dye solution

The dye stock solution (100 mg/L) was made with deionized water and methylene blue, then can be diluted with water to any desired concentration. A standard curve was generated by plotting the absorbance of various dye samples with known concentration.

2.4. Characterization

Fourier transform infrared spectroscopy (FTIR) (Perkin Elmer, L1860116) was used to characterize material structure performance. The surface morphology, size and element composition of samples were analyzed by scanning electron microscope (SEM) and energy dispersive X-ray spectroscopy (EDS). X-ray diffraction (XRD) (Bruker AXS Kappa APEX II CCD) be adopted to perform diffraction testing on powder

samples, providing the crystalline or amorphous properties. The MB concentration in liquid supernatant was monitored by an ultraviolet-visible spectrophotometer (Perkin Elmer, LAMBDA 1050) at 664 nm. Thermogravimetric analysis (TGA) was performed on a TA Instruments Hi-Red TGA 2950 thermogravimetric analyzer under nitrogen from 25□ to 700□ at 10□/min. The Brunauer-Emmett-Teller (BET) surface area and porosity of the samples were determined on accelerated surface area and porosimetry system (ASAP 2020, Global Spec.Inc., US).

The gel rate (G) of samples were investigated to confirm the occurrence of cross-linking reaction. Firstly, the dried sample was accurately weighed and represented as W_i. Afterwards, the sample was immersed in diethylene oxide for 48 h at room temperature with stirring. Finally, the sample was separated and dried at 60°C for 2 h before reweighing (W_f). G was calculated by the following formula:

$$G = \frac{W_f}{W_i} \times 100\% \qquad (1)$$

The water absorption of powder samples were measured by gravimetric method. To be specific, after vacuum drying to constant weight at 60°C, powder sample (Wi) was put in a weighing tea bag (W_j). Then it was soaked in distilled water for 24 h at room temperature. Taking out the tea bag and hanging until no water drips (about 10min), it was weighed on a balance again (W). The water absorption rate (M) was calculated according to equation (2). The empty tea bag was used as the blank control group to repeat the above experiment, and the gain in weight of empty tea bag was subtracted from the experiment result. To guarantee the reliability of data, the measurement result is averaged from three repetitive tests.

$$M = \frac{W - W_i - W_j}{W_i} \times 100\% \qquad (2)$$

2.5. Antibacterial activity assay

The gram-positive bacterium Staphylococcus aureus was chosen as the model to estimate antibacterial activity through contact-killing experiments. Briefly, the glass slide was coated with a thin and uniform layer of silica gel, followed by evenly coating the antibacterial sample powder on the silica gel. After drying, 18 μM Staphylococcus

aureus liquid slowly droped into it while covered with another clean glass slide. Afterwards, we placed it on the biological sterile incubate for 30 min at 37°C in an incubator. Whereafter, the two slides were separated with tweezers, put in a centrifuge tube and cautiously added water (10 mL). After manual shaking for a while, the centrifuge tube was agitated ultrasonically for 60 s. This process was repeated twice, whereupon the slide was taken out. 100 μM of the supernatant was collected to seed and incubated for overnight. Approximately 24 h later, the number of colonies was observed to study its antibacterial activity. For comparison, the blank group was treated in the same way as steps.

2.6. Adsorption experiments

Adsorption isotherm experiments were carried out by adding 10 mg sample to a series of 50 mL centrifuge tubes with MB solutions (10 mL, 5-40 mg/L) at pH 7. Then, the centrifuge tubes were sealed and separately shaken at different temperatures (30°C, 40°C, 50°C) for 24 h. The supernatant liquid was separated from sample by centrifugation. Finally, the residual MB concentration in the supernatant liquid was recorded on an ultraviolet-visible spectrophotometer at 664 nm.

Adsorption kinetics tests were performed by adding 10 mg sample to 50 mL centrifuge tubes with MB solutions (10 mL, 10 mg/L) at pH 7. Subsequently, the centrifuge tubes were sealed and stirred at 30°C. The supernatant liquid was taken at time intervals specified in advance and measured the MB concentration similarly to quantify the adsorption rate.

2.7. Desorption and reusability experiments

In the desorption test, ethanol was selected to desorb the dye in QAS-β-CDPU-20% for investigating the reusability. In general, the adsorbent (10 mg) was added to 10 mL of dye solution (40 mg/L). After stirring at room temperature for 24 h, the reaction mixture was subject to centrifugal separation to obtain precipitate and discard the supernatant. 10 mL of ethanol was added to the precipitate and continuously stirred for 24 h. Similarly, the suspension was centrifuged and collected the sediment for next

adsorbent recirculation. The dye concentration in the supernatant was measured by an ultraviolet-visible spectrophotometer, and each experiment above was conducted five consecutive adsorption-desorption cycles.

3. Results and discussion

3.1. Characterization of QAS-β-CDPU

3.1.1. FTIR analysis

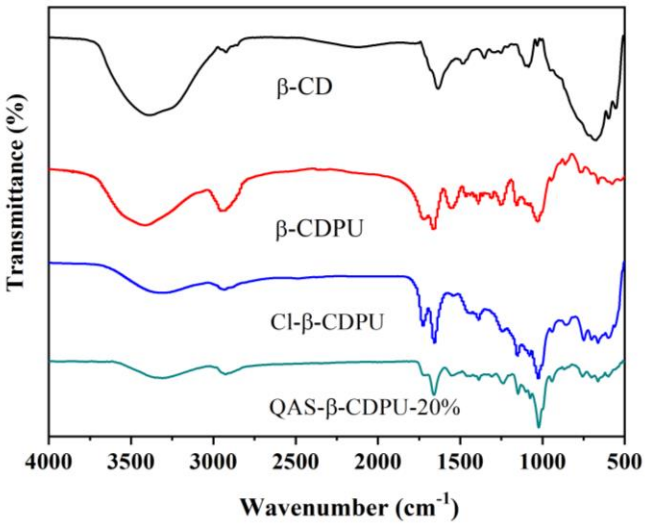

Fig. 1. FTIR spectra of β-CD, β-CDPU, Cl-β-CDPU and QAS-β-CDPU-20%.

To identify possible product structures, FTIR spectra of β-CD、β-CDPU、Cl-β-CDPU and QAS-β-CDPU-20% are shown in Fig. 1. The spectrum of β-CD exhibited two peaks at 3400 cm^{-1} and 2922 cm^{-1}, which are fitted with the stretching vibration of -OH and -CH_2-. In addition, two peaks located at 1031 cm^{-1} and 952 cm^{-1} are assigned to the antisymmetric glycosidic ν_a(C–O–C) vibrations and α-1,4-glycosidic bond stretching vibration [18,21], respectively. Compared with β-CD, the infrared spectrum of β-CDPU has apparent changes. The peak at 1155 cm^{-1} and 1440 cm^{-1} are severally corresponded to the stretching vibration of C-C/C-O and methylene. The peak at 1660 cm^{-1} and 1550cm^{-1} are attributed to stretching vibration of C=O and amide group [22]. The strong absorption peak around 1718 cm^{-1} is dominated by the stretching vibration of carbonyl of carbamate [23]. The disappearance of characteristic isocyanate peak at 2280 cm^{-1}, indicating the completion of polymerization reaction [24]. Furthermore, it

is clear to see stretching peaks of C-Cl at 857cm^{-1} in the spectrum of Cl-β-CDPU [25,26], which is the evidence of the polymerization. It is observed that the spectrum of QAS-β-CDPU-20% displayed five characteristic bands around 842 cm^{-1}, 1148cm^{-1}, 1460cm^{-1}, 1718cm^{-1} and 2988 cm^{-1}. The first one is in accordance with characteristic peak of C-Cl; the second one and the fourth one are attributable to the stretching vibration of C-C/C-O and the stretching vibration of carbonyl of carbamate; meanwhile, the rest of bands are assigned to characteristic peaks of quaternary ammonium salt [26]. The appearance of above peaks demonstrates the successful synthesis of QAS-β-CDPU-20%.

3.1.2. EDS and mapping analysis

EDS and mapping analysis (Fig. 2) reflected that C, O and Cl elements were uniformly distributed in the polymer material. Normally, there was supposed to be N element, rather than Pt element. This is mainly because synthetic polymer material is not conductive. To facilitate realistic testing, the surface of sample was sprayed with Pt to increase its conductivity. Unfortunately, since the content of N element is very low, the vast existence of Pt further influences the observation of N element. It is worth noting that the presence of Cl element indicates successful quaternarization for β-CDPU [27].

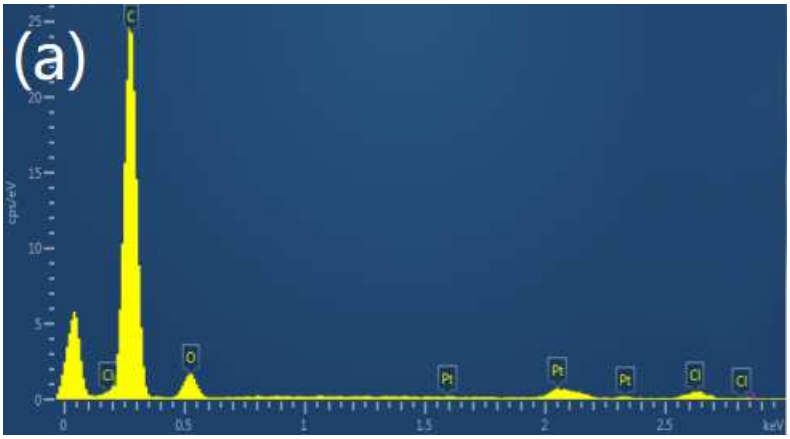

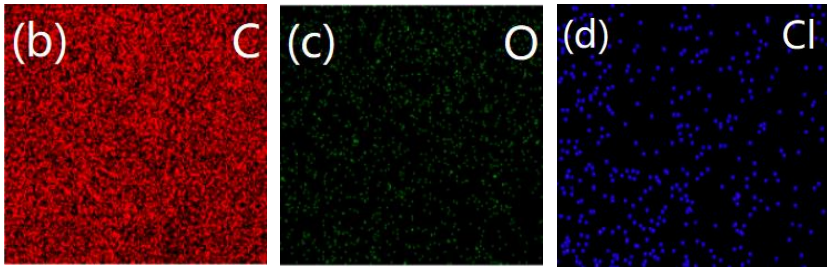

Fig. 2. EDS (a) and mapping images (b-d) of QAS-β-CDPU-20%.

3.1.3. Gel content and water absorption

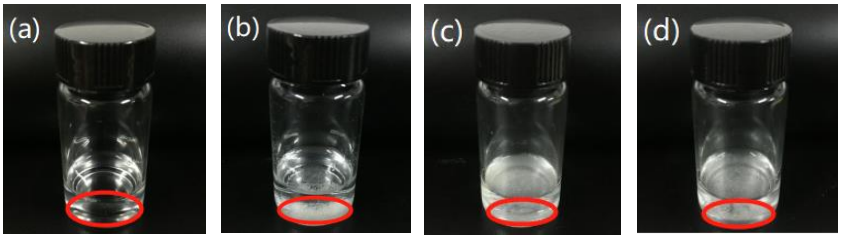

Fig. 3. (a) The solubility of β-CD in water and the solubility of QAS-β-CDPU-20% in (b) water, (c) HCl, (d) NaOH.

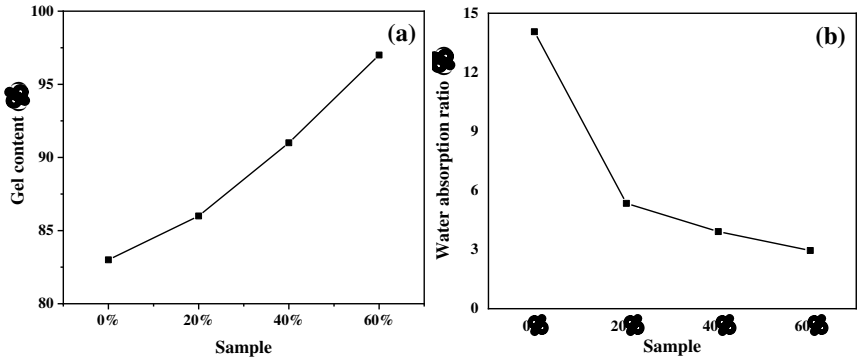

Fig. 4. (a) Gel rate and (b) water absorption rate of QAS-β-CDPU with different quaternization degrees.

Fig. 3 depicts the solubility of QAS-β-CDPU-20% in solvents. For pure β-CD (Fig. 3a), it is easily dissolved in water. By comparison, QAS-β-CDPU-20% is almost insoluble in water, HCl and NaOH (Fig. 3b-d), showing excellent solvent resistance. Additionally, the gel rate of QAS-β-CDPU with different quaternization degrees is shown in Fig. 4a. As the degree of quaternization rises, the gel rate of QAS-β-CDPU is a corresponding increase, which also has better solvent resistance. In fact, when the quaternization degree is higher, the amount of chlorine-containing monomers in the synthesis process is higher, causing rapid polymerization of β-CDPU and further cross-

linking of materials. As a result, the gel content of QAS-β-CDPU and the solvent resistance behavior reach maximum level. With regard to water absorption rate of QAS-β-CDPU, it gradually decreases with the increase of quaternization degree (Fig. 4b). The distance between the crosslinked points reduces along with the increase in cross-linking density. Thereby, the pore between the crosslinked points lose the ability to expand. Low volume porosity certainly results in low water absorption [28]. Besides, the swelling ability also relies on the presence of hydrophobic functional groups in its three-dimensional network. The formation of long chain alkyl groups on the backbone by means of quaternization utilizing TEA can improve hydrophobicity of QAS-β-CDPU. The hydrophobicity increases with increasing concentration of TEA [29].

3.1.4. SEM analysis

To gain an insight into the structure properties of β-CD and QAS-β-CDPU-20%, SEM analysis was conducted in Fig. 5. β-CD exhibits a thick flake structure with a clear edge, which is roughly rectangular in shape. On the contrary, QAS-β-CDPU-20% has almost no regular crystal structure [30].

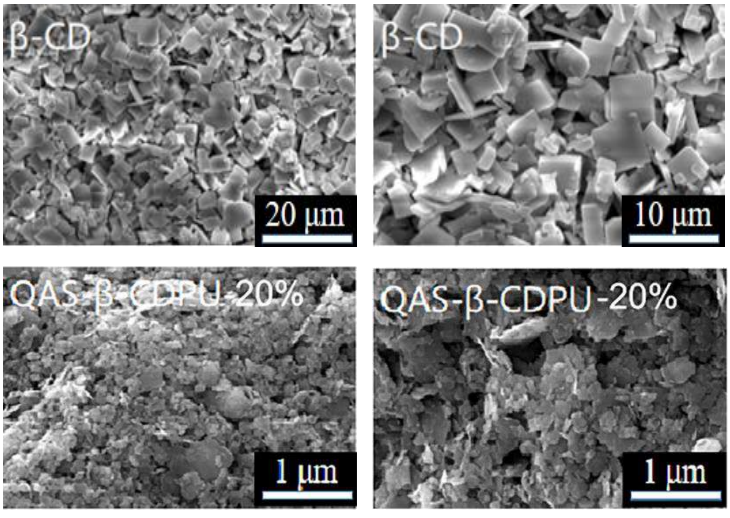

Fig. 5. SEM images of β-CD and QAS-β-CDPU-20%.

3.1.5. XRD analysis

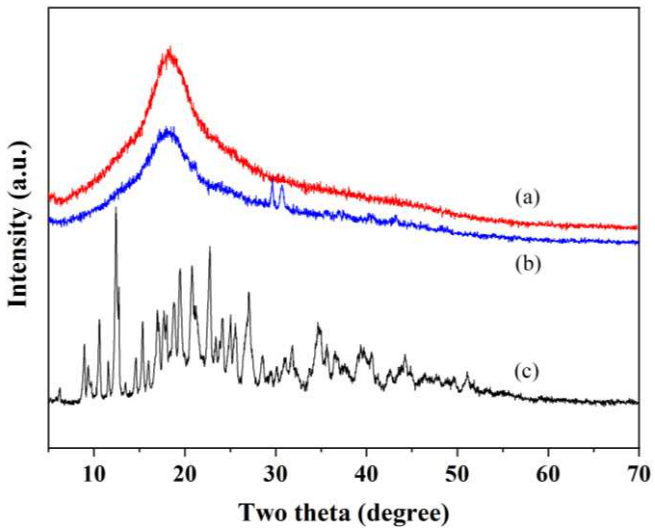

Fig. 6. XRD patterns of (a) QAS-β-CDPU-20%, (b) β-CDPU and (c) β-CD.

XRD analysis is able to characterize the phase purity and the structural effects related to the long-range order in polymer materials [31]. Fig. 6 describes XRD patterns of β-CD, β-CDPU and QAS-β-CDPU-20%. For β-CDPU and QAS-β-CDPU-20%, there is a broad band around 15°~20°, suggesting that they are amorphous in nature [18]. In contrast, the XRD pattern of pure β-CD presents many narrow peaks in range of 5-55°, confirming that it has good crystalline character. These results match well with the SEM images in Fig. 5. Since β-CD entered into PU backbone portion, its original crystal structure and internal hydrogen bonds were damaged [32]. Namely, the existence of PU backbone impeded the non-covalent interaction and filling efficiency of β-CD [33]. Therefore, the main specific diffraction peaks of β-CD disappeared in XRD pattern of β-CDPU.

XRD curves of β-CDPU and QAS-β-CDPU-20% have a very similar shape, the difference is that the peak intensity of QAS-β-CDPU-20% is weaker than β-CDPU. To some degree, this reflects a decrease in crystallinity due to the introduction of quaternary ammonium groups in QAS-β-CDPU-20%. Specifically, electrostatic repulsion by the positively charged trimethylammonium group in QAS-β-CDPU-20% may hinder the formation of inter-molecular and extra-molecular hydrogen bonds in β-CDPU backbone [34,35].

3.1.6. TGA analysis

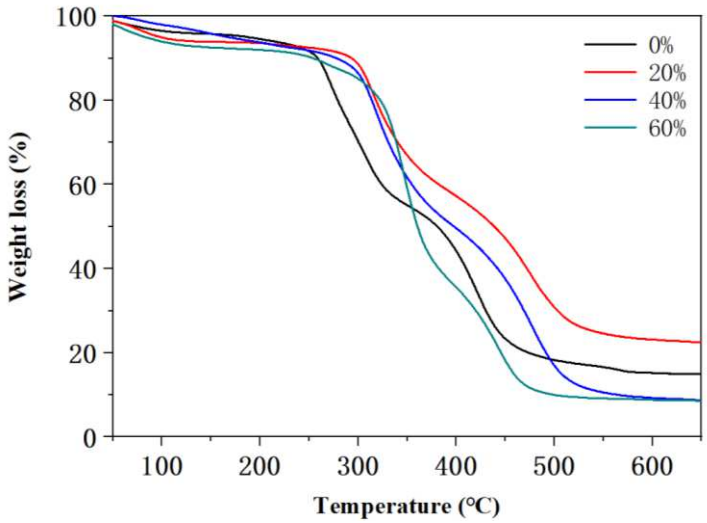

Fig. 7. TGA curves of QAS-β-CDPU with different quaternization degrees.

Fig. 7 shows TGA curves of QAS-β-CDPU with different quaternization degrees under a nitrogen atmosphere. All samples underwent about 5.5-8% weight loss at temperatures lower than 200°C, which was caused by evaporation of water adsorbed around the polymer skeleton (for instance, free water, physically adsorbed water, and bound water). As temperature rose, β-CDPU lost significant weight in the range of 260-320°C due to the destruction of β-CD [20]. When the temperature reached up to 300°C, the polyurethane moiety would decompose. It can be seen from Fig. 7 that β-CDPU was rapidly decomposed at 260°C. Samples after quaternization appeared a notable weight loss at a higher temperature of 300-310□. It reflects that the thermal stability of QAS-β-CDPU is better than β-CDPU [36].

3.1.7. BET analysis

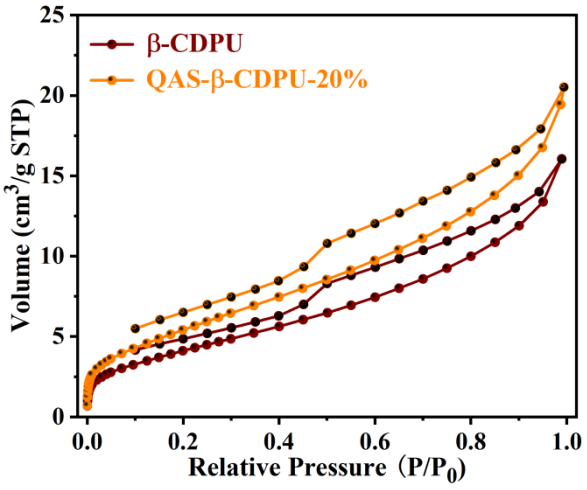

Fig. 8. N_2 adsorption-desorption isotherms of β-CDPU and QAS-β-CDPU-20%.

Table 1. The BET surface area, Barret-Joyner-Hallenda (BJH) adsorption cumulative volume of pores, adsorption average pore width for β-CD, β-CDPU and QAS-β-CDPU-20%.

Samples	BET Surface Area ($m^2 \cdot g^{-1}$)	BJH adsorption cumulative volume of pores ($cm^3 \cdot g^{-1}$)	Adsorption average pore width (nm)
β-CD	0.63	0.014	35.72
β-CDPU	15.56	3.575	0.95
QAS-β-CDPU-20%	20.57	4.727	0.95

Surface area is an important index to reflect adsorption capability of the adsorbent. Based on the International Union of Pure and Applied Chemistry (IUPAC) classification, N_2 adsorption-desorption isotherms of β-CDPU and QAS-β-CDPU-20% are analogous to the type II with H_3 hysteresis loop (Fig. 7). The specific area BET results in this study was measured using BET-type N_2 adsorption. By calculation and analysis (Table 1), the BET surface area and a total pore volume of QAS-β-CDPU-20% (20.57 $m^2 \cdot g^{-1}$, 4.727 $cm^3 \cdot g^{-1}$) are larger than β-CDPU (15.56 $m^2 \cdot g^{-1}$, 3.571 $cm^3 \cdot g^{-1}$), and both are superior to raw material β-CD (0.63 $m^2 \cdot g^{-1}$, 0.014 $cm^3 \cdot g^{-1}$). Owing to the amorphous structure, β-CDPU and QAS-β-CDPU-20% are more likely to form a microporous structure than the crystal structure of β-CD, resulting in a higher specific surface area [37]. In addition, the specific surface area was appearing to increase slightly after quaternary amine salt modification. Lima et al. also observed a slight increase in the BET surface area of quaternized coconut shell fibers [38]. Thamilarasi et al. found that the BET surface area of quaternized palm peel was lower than its raw material [39]. The discrepancy between the results is probably attributable to the different properties and composition of the materials concerned [40].

Of course, the specific surface area of β-CD or QAS-β-CDPU-20% is nothing compared to commercial activated carbon (CAC, 1100 $m^2 \cdot g^{-1}$) and commercial synthetic zeolite (450 $m^2 \cdot g^{-1}$) [41,42] Although the surface area of β-CD-based

polymers varied with different raw materials and preparation methods, a similar small surface area (0.11-8.01 $m^2 \cdot g^{-1}$) was seen in other studies [43]. Considering that the adsorption mechanism of β-CD to organic molecules is quite different from porous materials, surface area is not a critical factor for QAS-β-CDPU to adsorb MB [43].

3.2. Antibacterial activity

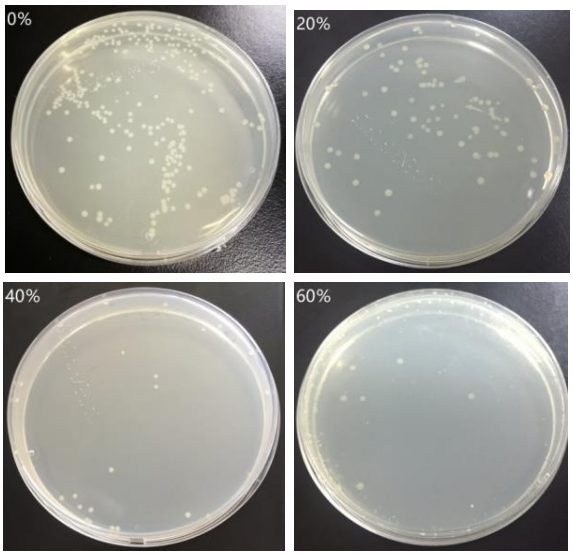

Fig. 9. Antibacterial activity of QAS-β-CDPU with different quaternization degrees against Staphylococcus aureus.

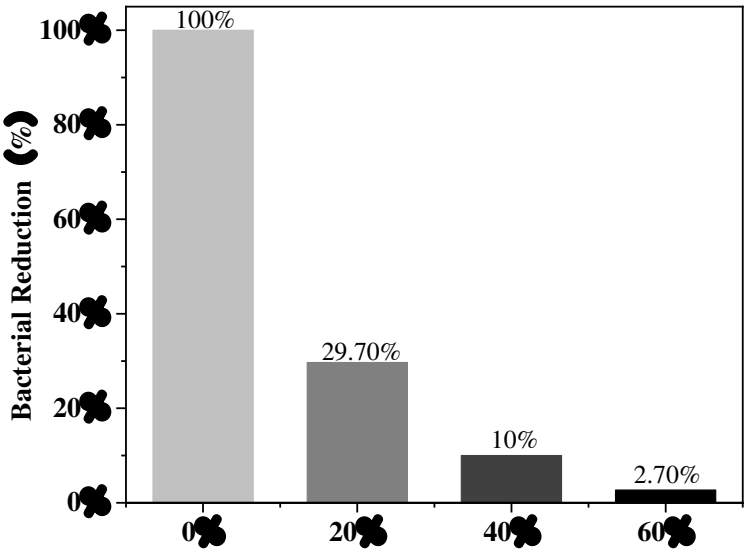

Fig. 10. Bacterial reduction of QAS-β-CDPU with different quaternization degrees against Staphylococcus aureus.

As is well-known, bacterial or fungal infections may lead to severe complications. Inadequate treatment for infected wounds can cause cellulitis (cell inflammation) and even fatal sepsis. Wound infection is likely the most frequent reason for substantial morbidity and mortality in extensive burns, trauma, and surgical operations. Therefore, preventing infection is vital to complete wound repair. Staphylococcus aureus, the most common microorganism for wound infection [44], was selected as model bacteria to study antibacterial properties of QAS-β-CDPU. As summarized in Fig. 9 and Fig. 10, all strains involving Staphylococcus aureus are well killed in the range of 70.3-97.3% when attaching the quaternary ammonium part to the cyclodextrin-polyurethane network. This definitely implies that QAS-β-CDPU has certain antibacterial ability. It can be noted that the number of Staphylococcus aureus decreased significantly with the increase of the quaternization concentration. QAS-β-CDPU with the highest quaternization concentration displayed almost 100% bacterial reduction against Staphylococcus aureus. Experiments show that the excellent bactericidal performance of QAS-β-CDPU was associated with quaternary ammonium salt groups on the surface. Refer to the relevant literature, the antibacterial activity of quaternary ammonium compounds benefit from its hydrophobicity [45,46]. The hydrophobic alkyl chain of the quaternary ammonium salt penetrates the bacterial membrane, causing the destruction of the membrane and the death of the bacteria [47]. The outstanding antibacterial properties of QAS-β-CDPU are conducive to the actual water treatment process, which can greatly reduce the use of disinfectants in the disinfection process, thereby saving costs and inhibiting by-products formation.

3.3. Adsorption properties

3.3.1. Adsorption kinetics

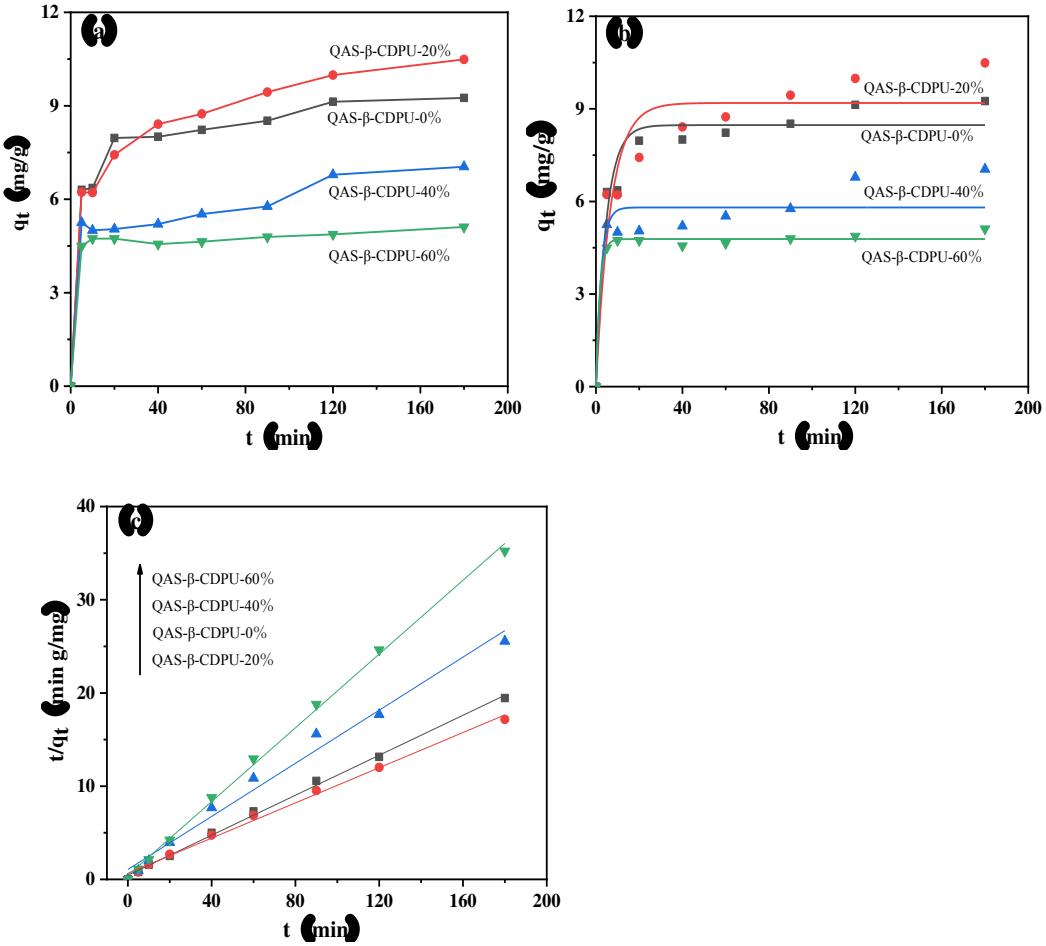

Fig. 11. (a) Variation in adsorption capacity with adsorption time for MB on QAS-β-CDPU with different quaternization degrees. (b) Pseudo-first-order and (c) pseudo-second-order models were used to evaluate the absorption kinetic. (temperature = 30□, absorbent dose = 0.01 g, neutral environment, MB concentration = 10 mg·L^{-1}).

Table 2. Adsorption kinetics parameters of MB on QAS-β-CDPU with different quaternization degrees.

Kinetic models	Equation	Sample	Parameters			
			K	Experimental qe (mg/g)	Calculated qe (mg/g)	R^2
Pseudo-first order	$q_t = q_{e1} - q_{e1}e^{-k_1 t}$	0%	0.209	9.253	8.473	0.9430
		20%	0.147	10.488	9.191	0.8924
		40%	0.410	7.043	5.806	0.8610
		60%	0.561	5.111	4.781	0.9893
Pseudo-second order	$\frac{t}{qt} = \frac{t}{q_{e2}} + \frac{1}{k_2 q^2_{e2}}$	0%	0.026	9.253	9.323	0.9973
		20%	0.014	10.488	10.595	0.9943
		40%	0.019	7.043	7.022	0.9834
		60%	0.090	5.111	5.054	0.9979

In adsorption research, adsorption kinetics are of great importance because they can describe the adsorption rate and provide valuable information for understanding the adsorption reaction mechanism [48]. Fig. 11a depicts the adsorption kinetics of methylene blue by QAS-β-CDPU. Pseudo-first-order and pseudo-second-order models were applied to evaluate the adsorption kinetics (Fig. 11b-c). The linear equations of these models are expressed as follows:

$$q_t = q_{e_1} - q_{e_1} e^{-k_1 t} \quad (3)$$

$$\frac{t}{q_t} = \frac{t}{q_{e_2}} + \frac{1}{k_2 q^2_{e_2}} \quad (4)$$

In equation(3), q_{e1} and q_t were separately the adsorption capacity (mg/g) at equilibrium and time t; k_1 was the rate constant of the pseudo-first-order model (min^{-1}). In equation(4), q_{e2} and q_t were the adsorption capacity (mg/g) at equilibrium and time t, respectively; k_2 was the rate constant of the pseudo-second-order model (g/mg/min).

Table 2 exhibits the adsorption kinetic parameters of QAS-β-CDPU with different quaternization degrees. Compared to the pseudo-first-order kinetic model, the pseudo-second-order kinetic model is more consistent with the experimental data. More precisely, the correlation coefficient (R^2) obtained from the pseudo-second-order kinetic model is greater than 0.99, and the degree of agreement between the calculated and experimental q_e value is higher. Fig. 10c represents a linear graph of t/qt versus t for MB adsorption on the prepared sample, confirming that chemical adsorption controls the adsorption rate. During the chemical adsorption process, the adsorbate was adsorbed on QAS-β-CDPU in the form of chemical bonds and further searched for adsorption sites, maximizing their coordination number with the surface [49]. Moreover, QAS-β-CDPU with 20% quaternization degree has a larger adsorption capacity for MB than β-CDPU. This may be attributed to the increased specific surface area and more active sites for adsorption. However, the adsorption effect was gradually weakened accompanied by a further increase in the proportion of quaternary amine salts. As a matter of fact, the quaternary ammonium salt is a cationic compound and MB is a cationic dye. With the continuous increase of quaternary ammonium salt, the positive

charge of the adsorbent continues to increase, generating a strong repulsive force for the same charges and then reducing adsorption effect.

3.3.2. Adsorption isotherms

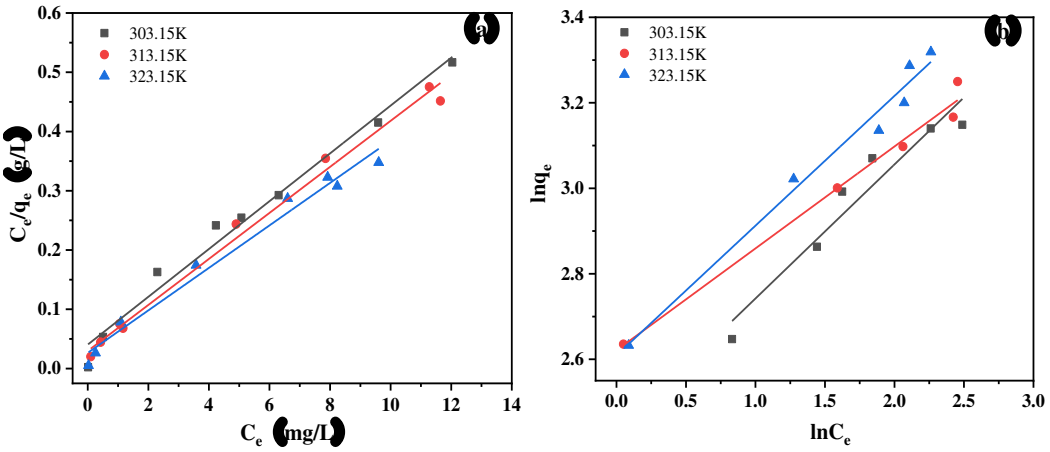

Fig. 12. Adsorption isotherm on QAS-β-CDPU-20% using (a) Langmuir and (b) Freundlich isotherm model under 303.15K, 313.15K and 323.15K. (incubating time = 24 h, absorbent dose = 0.01 g, neutral environment, MB concentration = 5-40 mg·L^{-1}).

Table 3. Adsorption isotherms parameters of MB on QAS-β-CDPU-20%.

Temperature	Langmuir				Freundlich		
	R^2	q_{max}	K_L	R_L	R^2	K_F	1/n
K		mg/g	L/mg			(mg/g)(mg/L)^n	
303.15	0.979	24.80	0.998	0.024-0.167	0.914	11.34	0.314
313.15	0.990	25.75	1.310	0.019-0.132	0.982	13.75	0.238
323.15	0.978	27.89	1.354	0.018-0.129	0.976	13.59	0.304

The adsorption isotherm can help us understand the distribution of adsorbed molecules between the liquid and solid phases and supply the most critical parameters for constructing an ideal adsorption model. It has been successfully used to describe the adsorption process [50]. On basis of Langmuir and Freundlich isotherm model, Fig. 12 reveals adsorption isotherm on QAS-β-CDPU-20% at 303.15K, 313.15K and 323.15K. The Langmuir model suggests that there is no interaction between adsorbed molecules, but just confined to a single layer on adsorbent surface. For Freundlich isotherm equation, it is a non-uniform surface adsorption based empirical model. The model

assumes that the strong binding sites are preferentially occupied, and the binding strength decreases as the degree of site occupation increases [51].These models is widely adopted for investigating the relationship between adsorption capacity of adsorbent and equilibrium adsorbent concentration in an aqueous solution.

The Langmuir and Freundlich isotherm equation are respectively defined below:

$$\frac{C_e}{q_e} = \frac{C_e}{q_{max}} + \frac{1}{q_{max} K_L} \quad (5)$$

$$\ln q_e = \frac{1}{n} \ln C_e + \ln K_F \quad (6)$$

Where C_e was the equilibrium concentration of MB in the solution (mg/L), q_e was the amount of MB adsorbed in equilibrium (mg/g), q_{max} was the theoretical maximum adsorption capacity (mg/g), K_L and K_F was Langmuir equilibrium constant and Freundlich constant, respectively. In the Freundlich equation, n is an index of adsorption intensity. The values of q_{max} and K_L can be obtained from the graph of C_e/q_e versus C_e (Fig. 12), while K_F and n can be determined from the graph of $\ln q_e$ versus $\ln C_e$.

The calculated fitting parameters are shown in Table 3. Overall,the Langmuir isotherm model provides a better fit to the experimental data, implying that the adsorption of MB is monolayer or homogeneous adsorption [49].The adsorption process is influenced by properties of dyes and adsorbents. Furthermore, separation factor, a dimensionless equilibrium parameter, is proposed to describe the essential characteristics of the Langmuir isotherm, specifically as follows:

$$R_L = \frac{1}{1 + K_L C_0} \quad (7)$$

In the formula, K_L is the Langmuir constant (L/mg), C_0 is the initial concentration of the dye (mg/L). This parameter indicates that the shape of the isotherm is unfavorable ($R_L>1$), favorable ($0<R_L<1$), linear ($R_L=1$) or irreversible ($R_L=0$) [52]. The calculated values of R_L (Table 3) are all in the range of 0-1, reflecting the favorable adsorption of MB by QAS-β-CDPU-20%. The introduction of β-CD into QAS-β-CDPU-20% material enables the cavity structure to capture organic molecules via the inclusion of host and guest. Additionally, the cyclodextrin-based carbamate network structure

formed by the reaction of β-CD and diisocyanate also contributes to adsorb dyes, so it has a dual advantage. The adsorption capacity increases with the increase of temperature, which illustrates high temperature is favorable for adsorption test.

3.3.3. Adsorption thermodynamics

Table 4. Adsorption thermodynamics parameters of MB on QAS-β-CDPU-20%.

ΔH^0	ΔS^0	ΔG^0 (KJ· mol^{-1})		
(KJ ·mol^{-1})	(J ·K^{-1})	303.15K	313.15K	323.15K
12.52	41.58	-0.08	-0.50	-0.92

The thermodynamics theory supposes that entropy change is a driving force in an isolated system where energy can be neither gained nor lost [53,54]. For further exploring the adsorption process, the the following equations (8-9) are used to deduce the changes in thermodynamic parameters, such as the standard Gibbs free energy change (ΔG^0), standard enthalpy change (ΔH^0) and standard entropy change (ΔS^0), etc. [55,56]:

$$\ln K_L = \frac{\Delta S^0}{R} - \frac{\Delta H^0}{RT} \quad (8)$$

$$\Delta G^0 = \Delta H^0 - T\Delta S^0 \quad (9)$$

Where K_L (L/mg) is the Langmuir isotherm constant, R (8.314 J·mol^{-1}·K^{-1}) is the universal gas constant ,and T (K) is the absolute temperature in Kelvin.

Table 4 lists the ΔG^0, ΔH^0 and ΔS^0 when MB was adsorbed on QAS-β-CDPU-20%. The positive value of ΔH^0 indicates that adsorption process is essentially endothermic [57]. This finding is in agreement with the result that the adsorption capacity of QAS-β-CDPU-20% for MB increases with increasing temperature. The negative ΔG^0 value and the positive ΔS^0 value demonstrate that the adsorption process is spontaneous.

3.3.4. Desorption and reusability

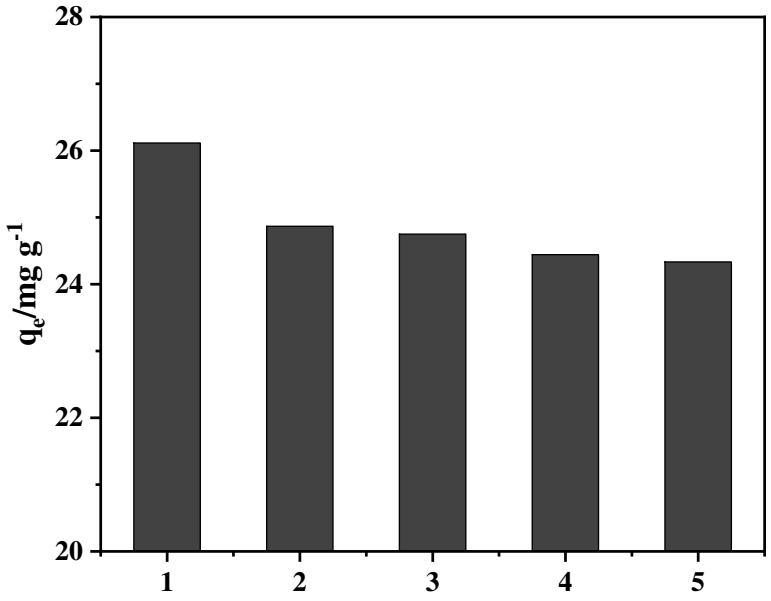

Fig. 13. Effect of recycle time of QAS-β-CDPU-20% on adsorption efficiency.

The recycling capacity of the adsorbent is the key element for its practical application. In the recycling experiment, QAS-β-CDPU-20% was washed with ethanol for 12 h under a shaker, and the effect of five consecutive adsorption-desorption cycles was studied (Fig. 13). Since MB might not completely desorb at elution step, the adsorption capacity decreased slowly in each subsequent cycle. Nevertheless, it can still achieve acceptable performance after five cycles. As it turned out, QAS-β-CDPU-20% can be recycled and reused for MB treatment.

4. Conclusion

In this paper, we successfully synthesized a series of QAS-β-CDPU for bacteria and dyes removal. Staphylococcus aureus was regarded as a model bacteria to assess antibacterial activity of polymer surface via contact sterilization experiments. QAS-β-CDPU with 60% quaternization degree has best antibacterial properties, up to 97.3% sterilization ratio. Meanwhile, QAS-β-CDPU shows superb adsorption performance for toxic carcinogenic MB as well. The related adsorption process was discussed in-depth, which is accord with pseudo-second-order kinetic model and Langmuir isotherm model. Furthermore, QAS-β-CDPU is insoluble in acid and alkali solvents, displaying excellent solvent resistance and stability. In view of above-

mentioned advantages, QAS-β-CDPU can be used as a multifunctional adsorbent for removing pathogens and chemical contaminates in wastewater disposal. It will be helpful for developing technologies related to field application and recycling.

Acknowledgement

This research was financially supported by the Science and Technology Research Projects of Lishui sci tech bureau (No. 2020GYX02), the Project of New Seedling Talents Program of Zhejiang Province (No. 2018R434004), the General Research Projects of Zhejiang Provincial Department of Education (No. Y201840153), Innovation and Entrepreneurship Program for college students in Zhejiang Province (No. S202010352036).

Conflicts of Interests

The authors declare that they have no conflict of interest.

References

1. Jain P, Pradeep T (2005) Potential of silver nanoparticle-coated polyurethane foam as an antibacterial water filter. Biotechnology and Bioengineering 90(1):59-63.
2. Diergaardt SM, Venter SN, Spreeth A, Theron J, Brözel VS (2004) The occurrence of campylobacters in water sources in south africa. Water Research 38(10):2589-2595.
3. Pernak J, Sobaszkiewicz K, Mirska I (2003) Anti-microbial activities of ionic liquids. Green Chemistry 5(1):52-56.
4. Fu Y, Wang F, Sheng H, Xu M, Liang Y, Bian Y, Hashsham SA, Jiang X, Tiedje JM (2020) Enhanced antibacterial activity of magnetic biochar conjugated quaternary phosphonium salt. Carbon 163:360-369.
5. Krasner SW, Weinberg HS, Richardson SD, Pastor SJ, Chinn R, Sclimenti MJ, Onstad GD, Thruston AD (2006) Occurrence of a new generation of disinfection

byproducts. Environmental Science & Technology 40(23):7175-7185.

6. Li Q, Mahendra S, Lyon DY, Brunet L, Liga MV, Li D, Alvarez PJJ (2008) Antimicrobial nanomaterials for water disinfection and microbial control: Potential applications and implications. Water Research 42(18):4591-4602.
7. He W, Zhang Y, Luo F, Li J, Wang K, Tan H, Fu Q (2015) A novel non-releasing antibacterial poly(styrene-acrylate)/waterborne polyurethane composite containing gemini quaternary ammonium salt. RSC Advances 5(109):89763-89770.
8. Chang L, Zhang X, Shi X, Zhao L, Liu X (2014) Preparation and characterization of a novel antibacterial fiber modified by quaternary phosphonium salt on the surface of polyacrylonitrile fiber. Fibers and Polymers 15(10):2026-2031.
9. Freiberg S, Zhu XX (2004) Polymer microspheres for controlled drug release. International Journal of Pharmaceutics 282(1):1-18.
10. Lei Y, Zhou S, Dong C, Zhang A, Lin Y (2018) Pdms tri-block copolymers bearing quaternary ammonium salts for epidermal antimicrobial agents: Synthesis, surface adsorption and non-skin-penetration. Reactive and Functional Polymers 124:20-28.
11. Badruddoza AZM, Hazel GSS, Hidajat K, Uddin MS (2010) Synthesis of carboxymethyl-β-cyclodextrin conjugated magnetic nano-adsorbent for removal of methylene blue. Colloids and Surfaces A: Physicochemical and Engineering Aspects 367(1):85-95.
12. Crini G (2005) Recent developments in polysaccharide-based materials used as adsorbents in wastewater treatment. Progress in Polymer Science 30(1):38-70.
13. Szejtli J (1998) Introduction and general overview of cyclodextrin chemistry. Chemical Reviews 98(5):1743-1754.
14. Ozmen EY, Sezgin M, Yilmaz A, Yilmaz M (2008) Synthesis of β-cyclodextrin and starch based polymers for sorption of azo dyes from aqueous solutions. Bioresource Technology 99(3):526-531.
15. Guo Y, Guo S, Ren J, Zhai Y, Dong S, Wang E (2010) Cyclodextrin

functionalized graphene nanosheets with high supramolecular recognition capability: Synthesis and host−guest inclusion for enhanced electrochemical performance. ACS Nano 4(7):4001-4010.

16. Wang H, Liu Y-g, Zeng G-m, Hu X-j, Hu X, Li T-t, Li H-y, Wang Y-q, Jiang L-h (2014) Grafting of β-cyclodextrin to magnetic graphene oxide via ethylenediamine and application for cr(vi) removal. Carbohydrate Polymers 113:166-173.
17. Leudjo Taka A, Pillay K, Yangkou Mbianda X (2017) Nanosponge cyclodextrin polyurethanes and their modification with nanomaterials for the removal of pollutants from waste water: A review. Carbohydrate Polymers 159:94-107.
18. Nasiri S, Alizadeh N (2019) Synthesis and adsorption behavior of hydroxypropyl-β-cyclodextrin–polyurethane magnetic nanoconjugates for crystal and methyl violet dyes removal from aqueous solutions. RSC Advances 9(42):24603-24616.
19. Nurdin N, Helary G, Sauvet G (1993) Biocidal polymers active by contact. Ii. Biological evaluation of polyurethane coatings with pendant quaternary ammonium salts. Journal of Applied Polymer Science 50(4):663-670.
20. Zhao J, Liu T-T, Chen G (2016) An effective β-cyclodextrin polyurethane spherical adsorbent for the chromatographic enrichment of corilagin from phyllanthus niruri l. Extract. Reactive and Functional Polymers 102:119-129.
21. Yan J, Zhu Y, Qiu F, Zhao H, Yang D, Wang J, Wen W (2016) Kinetic, isotherm and thermodynamic studies for removal of methyl orange using a novel β-cyclodextrin functionalized graphene oxide-isophorone diisocyanate composites. Chemical Engineering Research and Design 106:168-177.
22. Liang Q, Chai K, Lu K, Xu Z, Li G, Tong Z, Ji H (2017) Theoretical and experimental studies on the separation of cinnamyl acetate and cinnamaldehyde by adsorption onto a β-cyclodextrin polyurethane polymer. RSC Advances 7(69):43502-43511.
23. Dong K, Qiu F, Guo X, Xu J, Yang D, He K (2013) Adsorption behavior of azo dye eriochrome black t from aqueous solution by β-cyclodextrins/polyurethane

foam material. Polymer-Plastics Technology and Engineering 52(5):452-460.

24. Kiasat AR, Nazari S (2012) Application of β-cyclodextrin-polyurethane as a stationary microvessel and solid–liquid phase-transfer catalyst: Preparation of benzyl cyanides and azides in water. Catalysis Communications 18:102-105.

25. Soman VV, Kelkar DS (2009) Ftir studies of doped pmma - pvc blend system. Macromolecular Symposia 277(1):152-161.

26. Kenawy E-R, Abdel-Hay FI, El-Magd AA, Mahmoud Y (2006) Biologically active polymers: Vii. Synthesis and antimicrobial activity of some crosslinked copolymers with quaternary ammonium and phosphonium groups. Reactive and Functional Polymers 66(4):419-429.

27. Wang W, Chen Z, Zhou H, Zhang Y, Wang X (2018) Two-dimensional lamellar magnesium silicate with large spacing as an excellent adsorbent for uranium immobilization. Environmental Science: Nano 5(10):2406-2414.

28. Sarmah D, Karak N (2020) Biodegradable superabsorbent hydrogel for water holding in soil and controlled-release fertilizer. Journal of Applied Polymer Science 137(13):48495.

29. Sarmah D, Karak N (2020) Double network hydrophobic starch based amphoteric hydrogel as an effective adsorbent for both cationic and anionic dyes. Carbohydrate Polymers 242:116320.

30. Gao S, Liu Y, Jiang J, Ji Q, Fu Y, Zhao L, Li C, Ye F (2019) Physicochemical properties and fungicidal activity of inclusion complexes of fungicide chlorothalonil with β-cyclodextrin and hydroxypropyl-β-cyclodextrin. Journal of Molecular Liquids 293:111513.

31. Mohamed MH, Wilson LD, Headley JV (2015) Tuning the physicochemical properties of β-cyclodextrin based polyurethanes via cross-linking conditions. Microporous and Mesoporous Materials 214:23-31.

32. Ye H, Wang J, Chen X, Shi S-P (2013) Novel modification of pu membranes by cyclodextrin (cd) crosslinking for simultaneously improving selectivity and permeability. Journal of Macromolecular Science, Part A 50(6):661-669.

33. Mele A, Castiglione F, Malpezzi L, Ganazzoli F, Raffaini G, Trotta F, Rossi B,

Fontana A, Giunchi G (2011) Hr mas nmr, powder xrd and raman spectroscopy study of inclusion phenomena in βcd nanosponges. Journal of Inclusion Phenomena and Macrocyclic Chemistry 69(3):403-409.

34. Gonil P, Sajomsang W, Ruktanonchai UR, Pimpha N, Sramala I, Nuchuchua O, Saesoo S, Chaleawlert-umpon S, Puttipipatkhachorn S (2011) Novel quaternized chitosan containing β-cyclodextrin moiety: Synthesis, characterization and antimicrobial activity. Carbohydrate Polymers 83(2):905-913.
35. Chaleawlert-umpon S, Nuchuchua O, Saesoo S, Gonil P, Ruktanonchai UR, Sajomsang W, Pimpha N (2011) Effect of citrate spacer on mucoadhesive properties of a novel water-soluble cationic β-cyclodextrin-conjugated chitosan. Carbohydrate Polymers 84(1):186-194.
36. Zhang D, Xie J, Yu P, Huang X, Yang M, Liu H (2012) Antifungal activity and humidity sensitivity of quaternized cellulose synthesized in naoh/urea aqueous solution. Cellulose 19(1):189-198.
37. Guo S, Han S, Mao H, Dong S, Wu C, Jia L, Chi B, Pu J, Li J (2014) Structurally controlled zno/tio2 heterostructures as efficient photocatalysts for hydrogen generation from water without noble metals: The role of microporous amorphous/crystalline composite structure. Journal of Power Sources 245:979-985.
38. de Lima ACA, Nascimento RF, de Sousa FF, Filho JM, Oliveira AC (2012) Modified coconut shell fibers: A green and economical sorbent for the removal of anions from aqueous solutions. Chemical Engineering Journal 185-186:274-284.
39. Thamilarasi MJV, Anilkumar P, Theivarasu C, Sureshkumar MV (2018) Removal of vanadium from wastewater using surface-modified lignocellulosic material. Environmental Science and Pollution Research 25(26):26182-26191.
40. Zhang R, Leiviskä T (2020) Surface modification of pine bark with quaternary ammonium groups and its use for vanadium removal. Chemical Engineering Journal 385:123967.

41. Al-Degs Y, Khraisheh MAM, Allen SJ, Ahmad MN (2000) Effect of carbon surface chemistry on the removal of reactive dyes from textile effluent. Water Research 34(3):927-935.
42. Chutia P, Kato S, Kojima T, Satokawa S (2009) Arsenic adsorption from aqueous solution on synthetic zeolites. Journal of Hazardous Materials 162(1):440-447.
43. Hu Q, Gao D-W, Pan H, Hao L, Wang P (2014) Equilibrium and kinetics of aniline adsorption onto crosslinked sawdust-cyclodextrin polymers. RSC Advances 4(75):40071-40077.
44. Gharibi R, Yeganeh H, Rezapour-Lactoee A, Hassan ZM (2015) Stimulation of wound healing by electroactive, antibacterial, and antioxidant polyurethane/siloxane dressing membranes: In vitro and in vivo evaluations. ACS Applied Materials & Interfaces 7(43):24296-24311.
45. Jennings MC, Minbiole KPC, Wuest WM (2015) Quaternary ammonium compounds: An antimicrobial mainstay and platform for innovation to address bacterial resistance. ACS Infectious Diseases 1(7):288-303.
46. Inta O, Yoksan R, Limtrakul J (2014) Hydrophobically modified chitosan: A bio-based material for antimicrobial active film. Materials Science and Engineering: C 42:569-577.
47. Song J, Kong H, Jang J (2011) Bacterial adhesion inhibition of the quaternary ammonium functionalized silica nanoparticles. Colloids and Surfaces B: Biointerfaces 82(2):651-656.
48. Chen R, Yu J, Xiao W (2013) Hierarchically porous mno2 microspheres with enhanced adsorption performance. Journal of Materials Chemistry A 1(38):11682-11690.
49. Zeng A, Zeng A (2017) Synthesis of a quaternized beta cyclodextrin-montmorillonite composite and its adsorption capacity for cr(vi), methyl orange, and p-nitrophenol. Water, Air, & Soil Pollution 228(8):278.
50. Liu J, Liu G, Liu W (2014) Preparation of water-soluble β-cyclodextrin/poly(acrylic acid)/graphene oxide nanocomposites as new

adsorbents to remove cationic dyes from aqueous solutions. Chemical Engineering Journal 257:299-308.

51. Lei C, Zhu X, Zhu B, Jiang C, Le Y, Yu J (2017) Superb adsorption capacity of hierarchical calcined ni/mg/al layered double hydroxides for congo red and cr(vi) ions. Journal of Hazardous Materials 321:801-811.

52. Vahedi S, Tavakoli O, Khoobi M, Ansari A, Ali Faramarzi M (2017) Application of novel magnetic β-cyclodextrin-anhydride polymer nano-adsorbent in cationic dye removal from aqueous solution. Journal of the Taiwan Institute of Chemical Engineers 80:452-463.

53. Badruddoza AZM, Tay ASH, Tan PY, Hidajat K, Uddin MS (2011) Carboxymethyl-β-cyclodextrin conjugated magnetic nanoparticles as nano-adsorbents for removal of copper ions: Synthesis and adsorption studies. Journal of Hazardous Materials 185(2):1177-1186.

54. Fan J, Cai W, Yu J (2011) Adsorption of n719 dye on anatase tio2 nanoparticles and nanosheets with exposed (001) facets: Equilibrium, kinetic, and thermodynamic studies. Chemistry-An Asian Journal 6(9):2481-2490.

55. Garcia-Delgado RA, Cotoruelo-Minguez LM, Rodriguez JJ (1992) Equilibrium study of single-solute adsorption of anionic surfactants with polymeric xad resins. Separation Science and Technology 27(7):975-987.

56. Qiu T, Zeng Y, Ye C, Tian H (2012) Adsorption thermodynamics and kinetics of p-xylene on activated carbon. Journal of Chemical and Engineering Data 57(5):1551-1556.

57. Fan L, Luo C, Sun M, Qiu H, Li X (2013) Synthesis of magnetic beta-cyclodextrin-chitosan/graphene oxide as nanoadsorbent and its application in dye adsorption and removal. Colloids and Surfaces B-Biointerfaces 103:601-607.

Figures

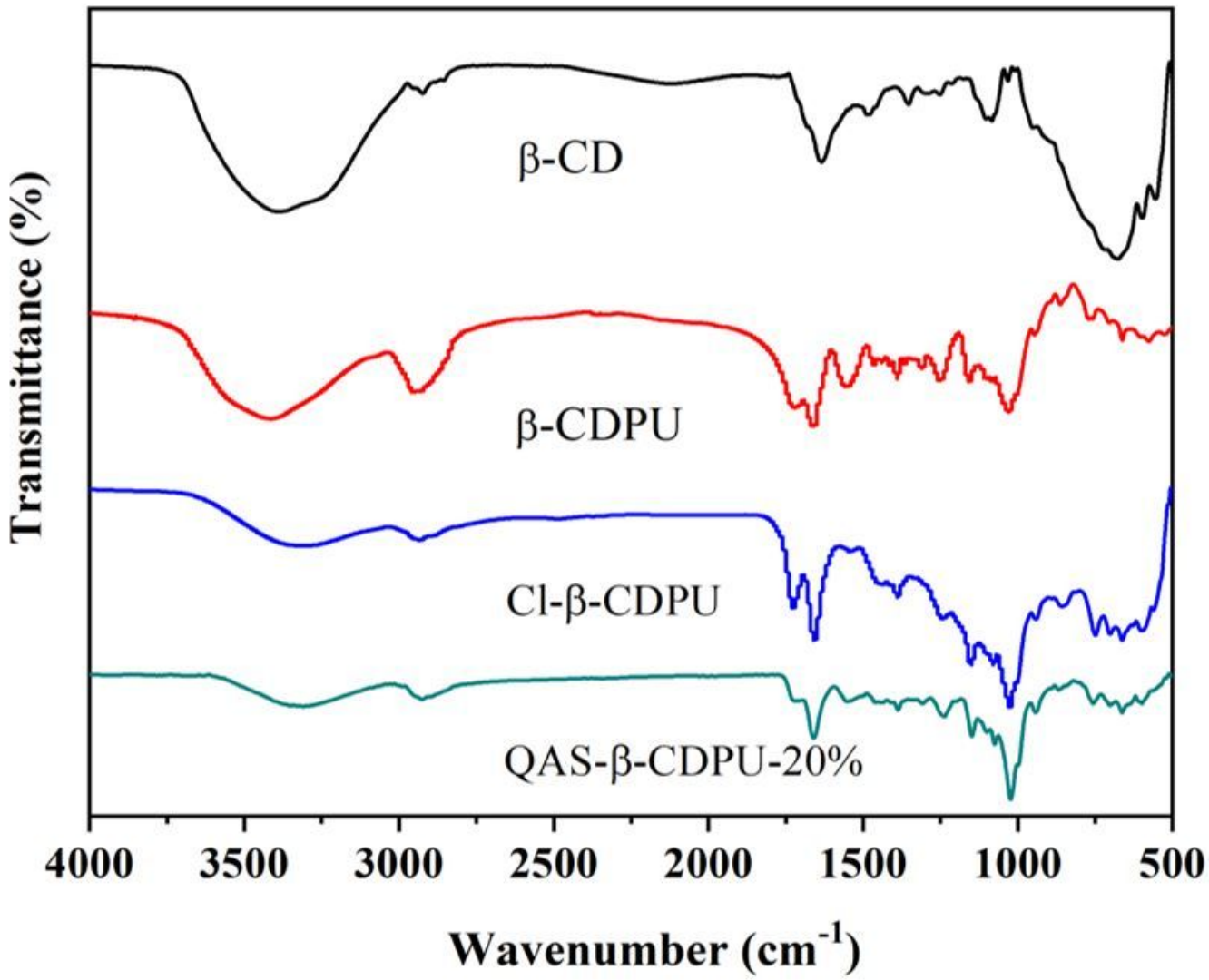

Figure 1

FTIR spectra of β-CD, β-CDPU, Cl-β-CDPU and QAS-β-CDPU-20%.

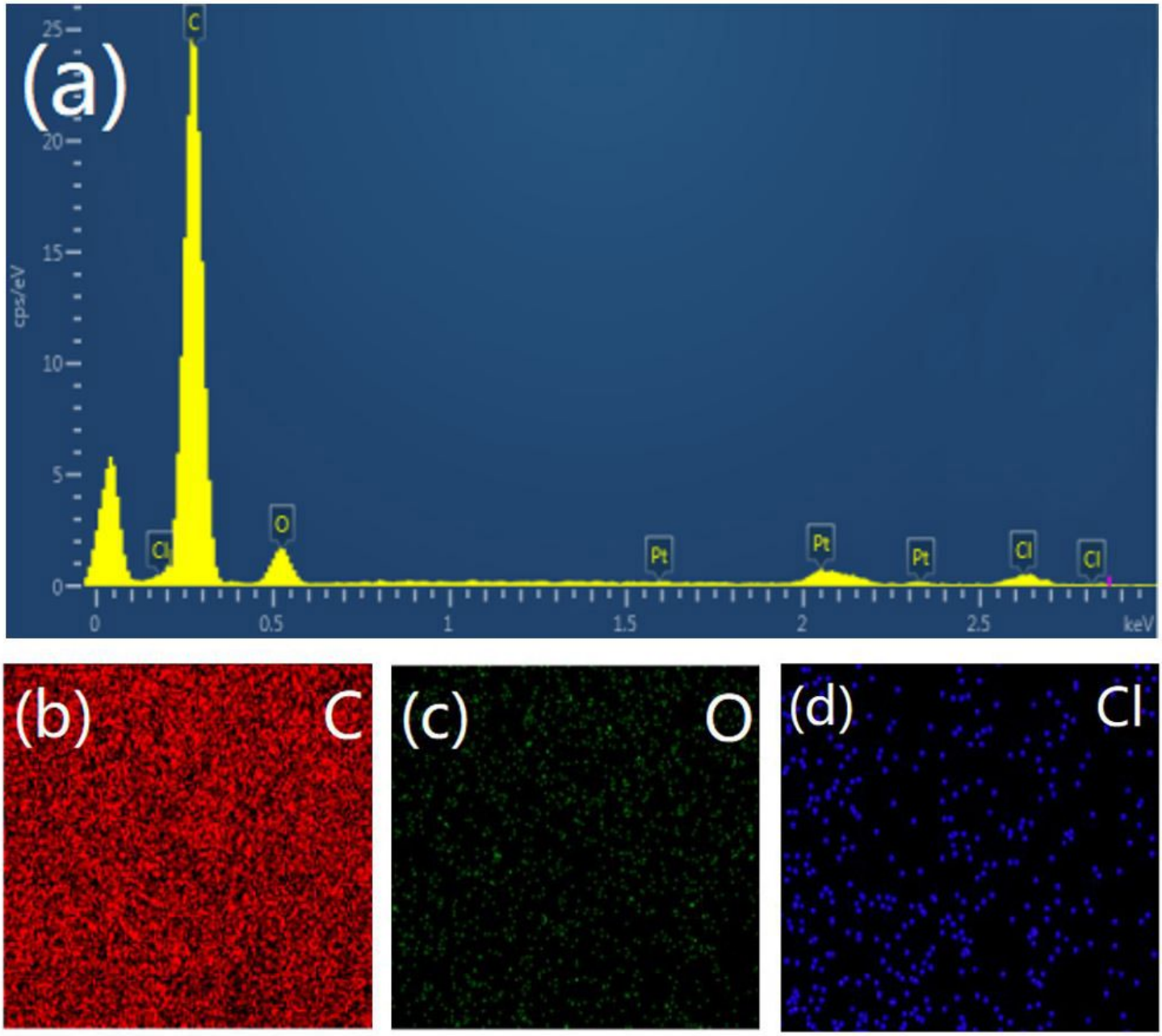

Figure 2

EDS (a) and mapping images (b-d) of QAS-β-CDPU-20%.

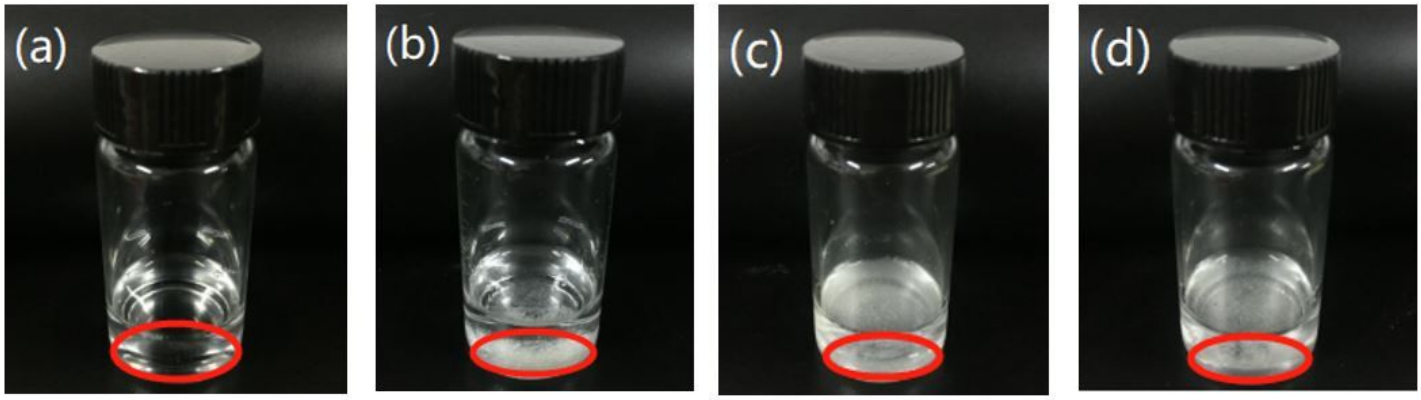

Figure 3

(a) The solubility of β-CD in water and the solubility of QAS-β-CDPU-20% in (b) water, (c) HCl, (d) NaOH.

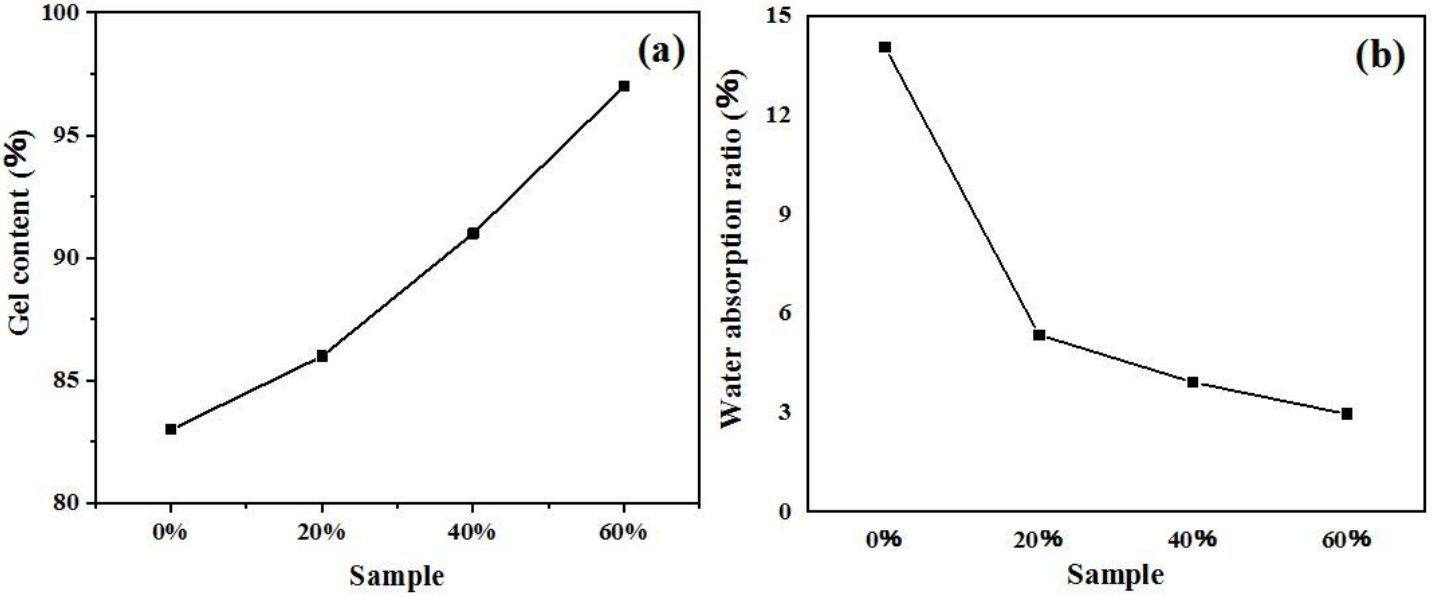

Figure 4

(a) Gel rate and (b) water absorption rate of QAS-β-CDPU with different quaternization degrees.

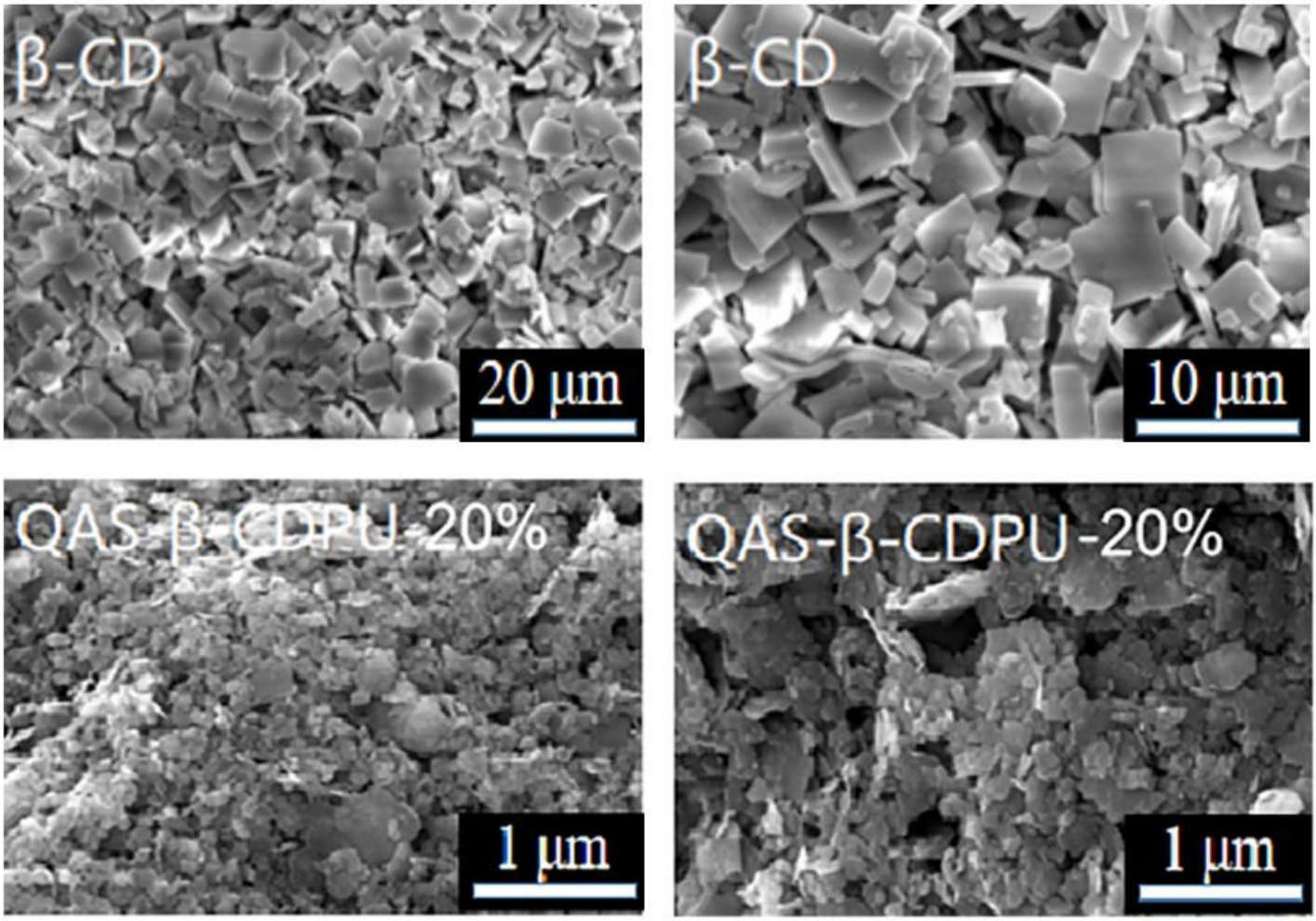

Figure 5

SEM images of β-CD and QAS-β-CDPU-20%.

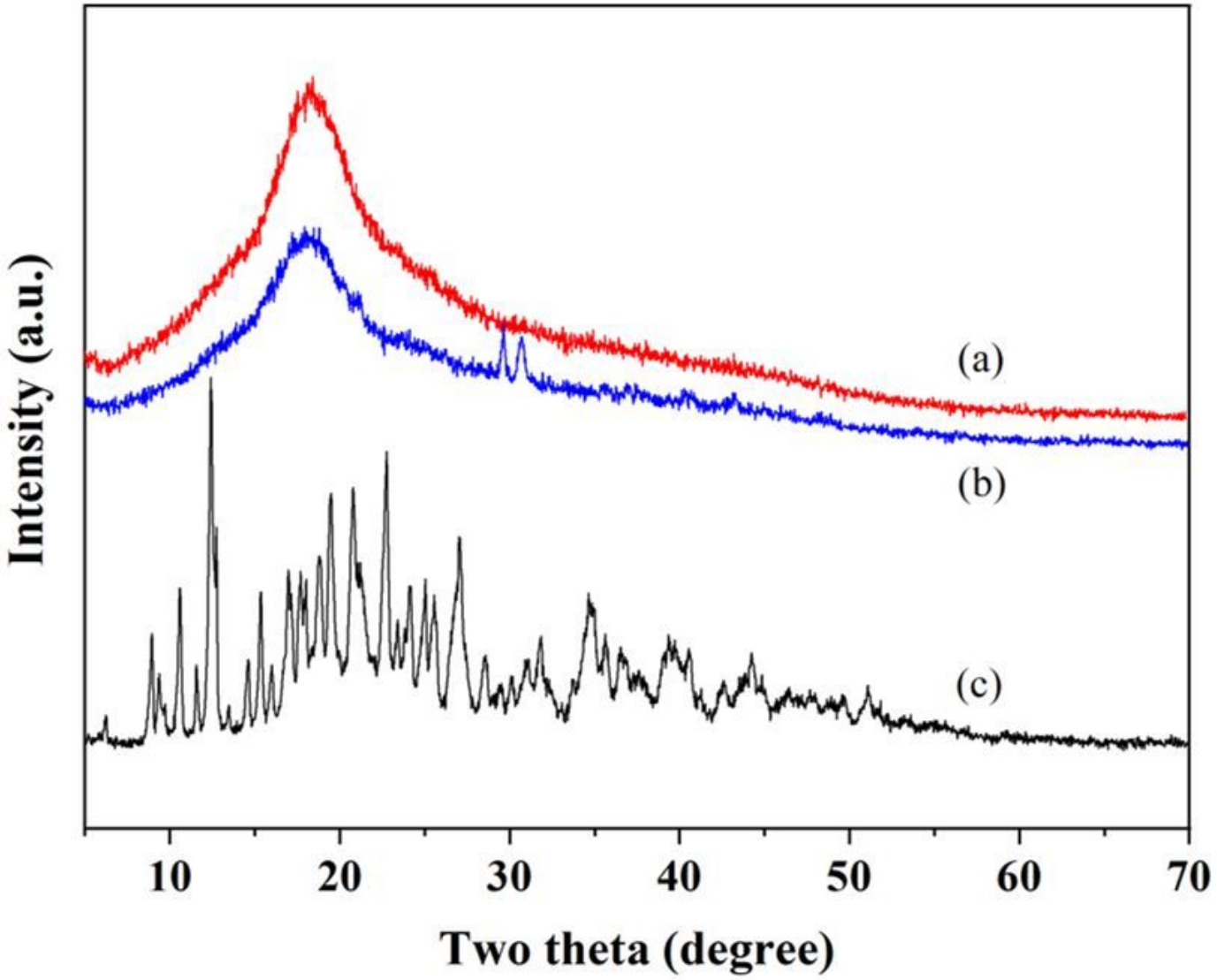

Figure 6

XRD patterns of (a) QAS-β-CDPU-20%, (b) β-CDPU and (c) β-CD.

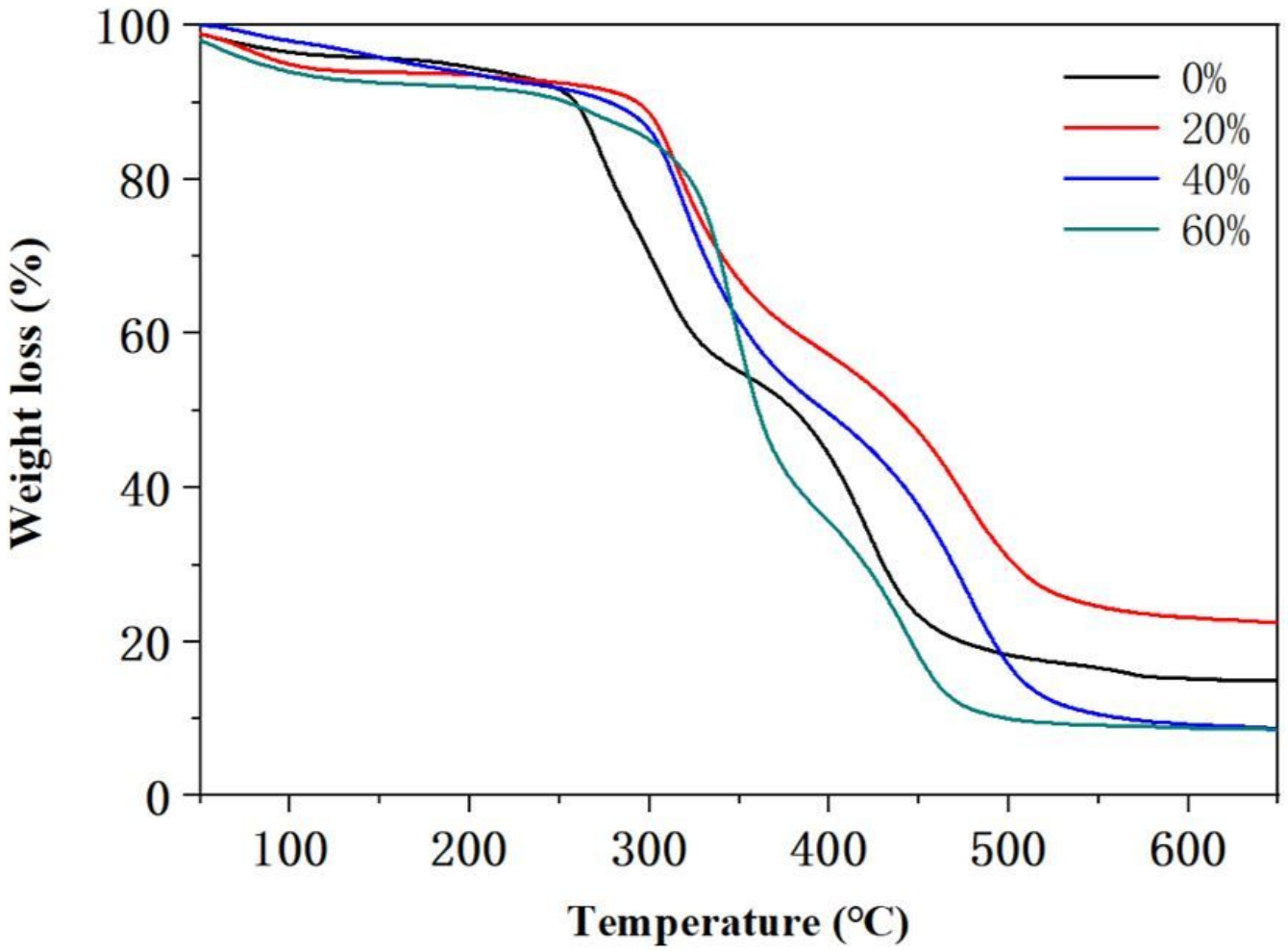

Figure 7

TGA curves of QAS-β-CDPU with different quaternization degrees.

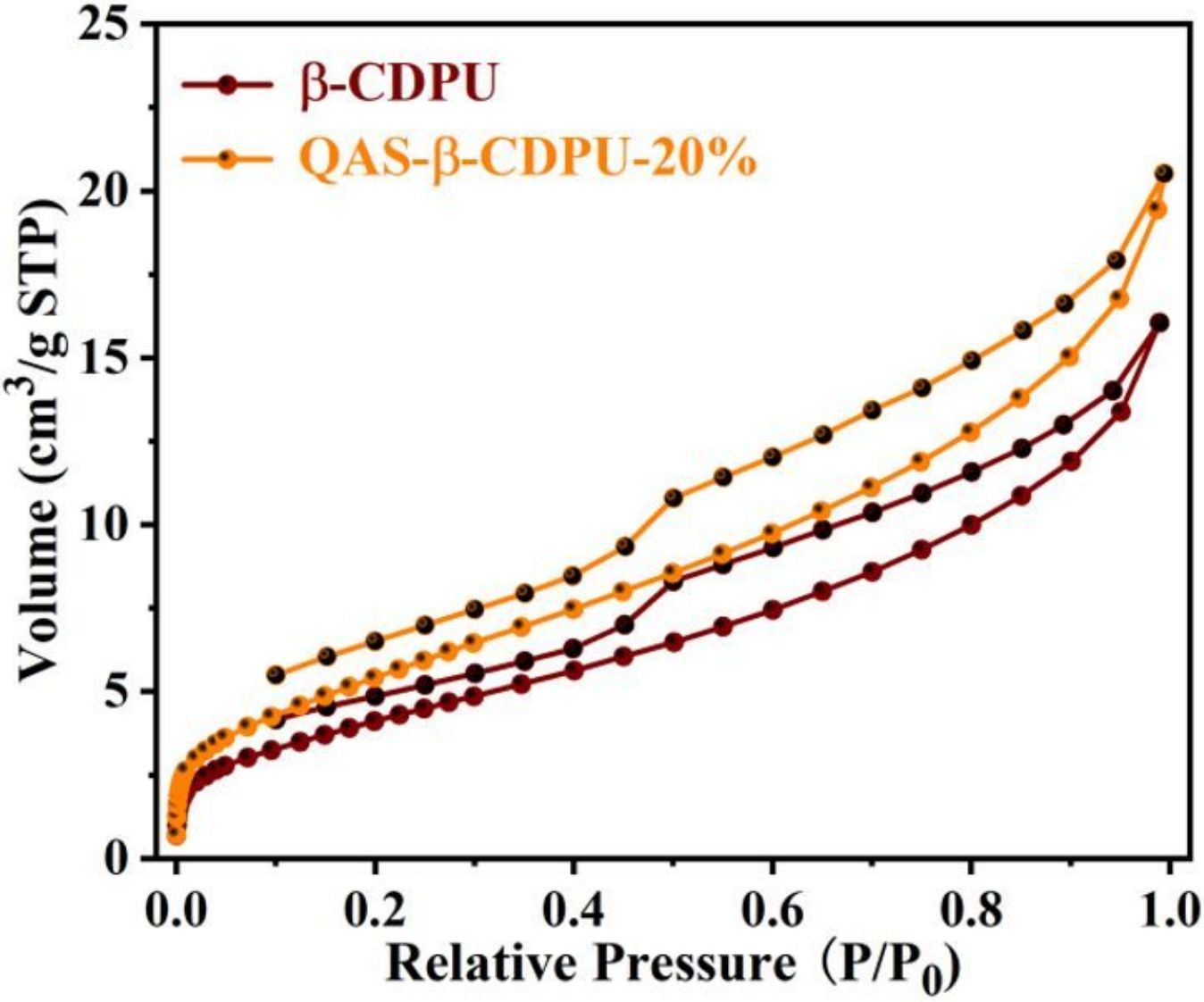

Figure 8

N2 adsorption-desorption isotherms of β-CDPU and QAS-β-CDPU-20%.

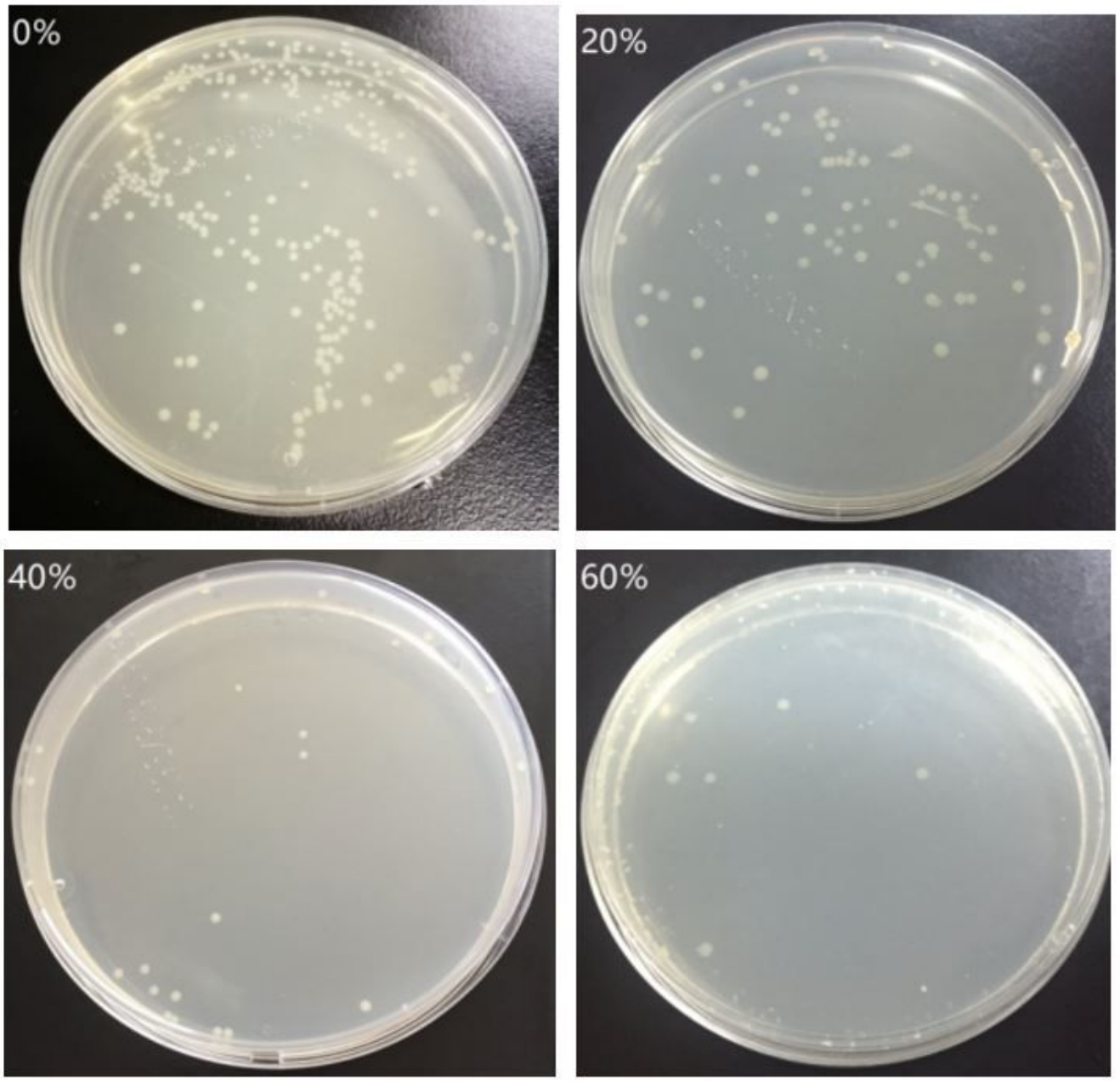

Figure 9

Antibacterial activity of QAS-β-CDPU with different quaternization degrees against Staphylococcus aureus.

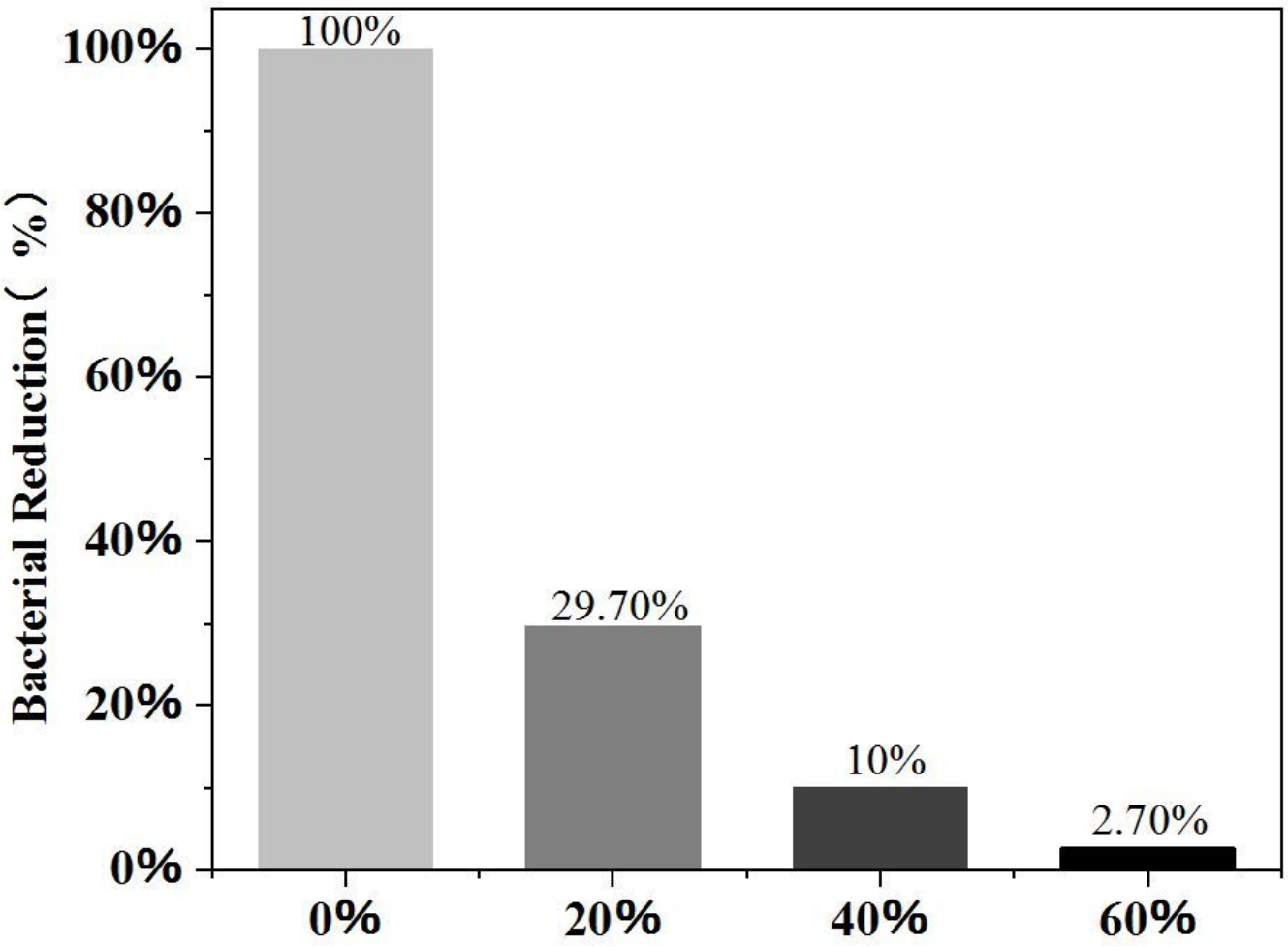

Figure 10

Bacterial reduction of QAS-β-CDPU with different quaternization degrees against Staphylococcus aureus.

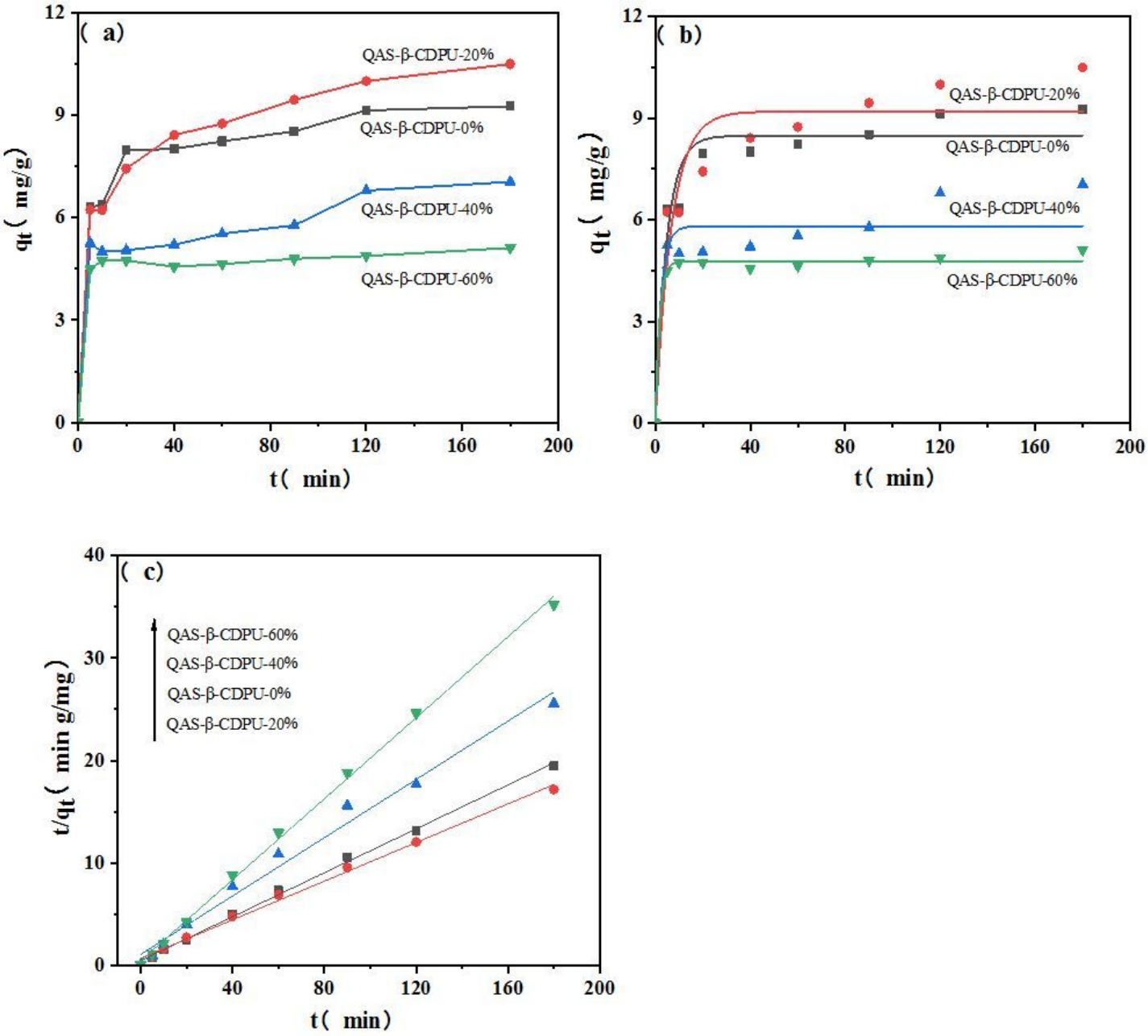

Figure 11

(a) Variation in adsorption capacity with adsorption time for MB on QAS-β-CDPU with different quaternization degrees. (b) Pseudo-first-order and (c) pseudo-second-order models were used to evaluate the absorption kinetic. (temperature = 30□, absorbent dose = 0.01 g, neutral environment, MB concentration = 10 mg·L-1).

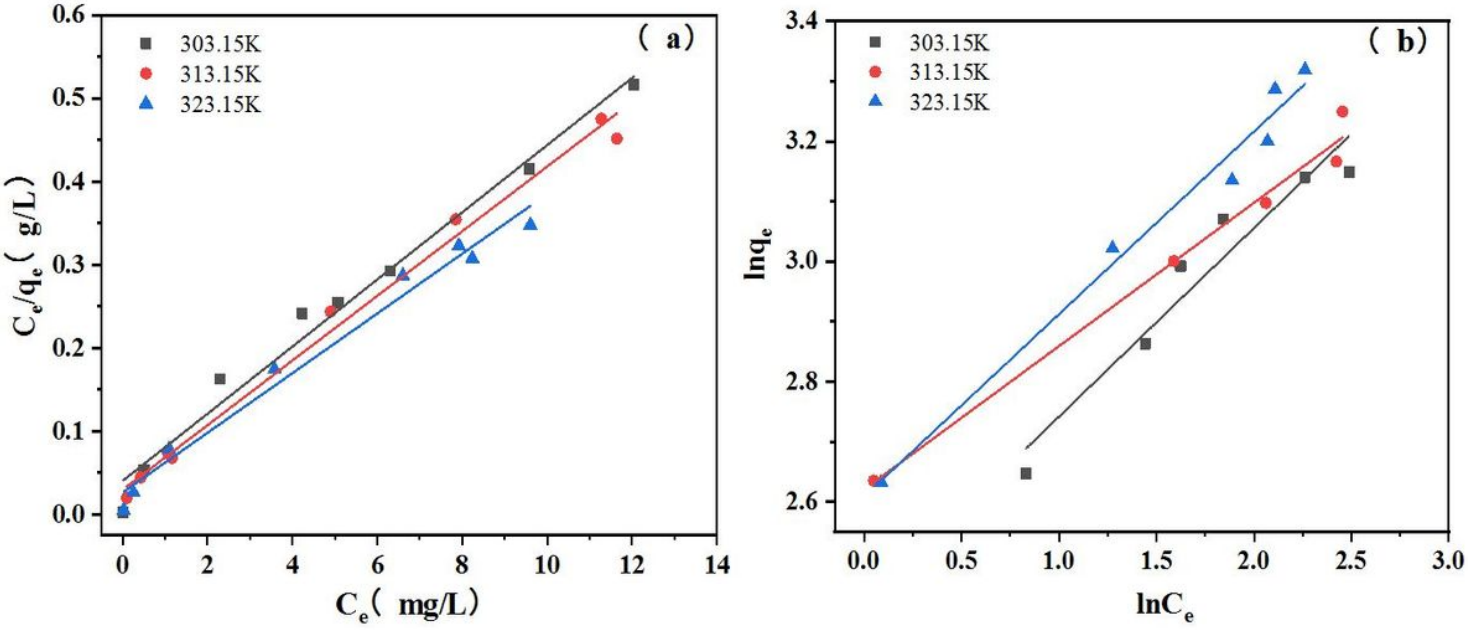

Figure 12

Adsorption isotherm on QAS-β-CDPU-20% using (a) Langmuir and (b) Freundlich isotherm model under 303.15K, 313.15K and 323.15K. (incubating time = 24 h, absorbent dose = 0.01 g, neutral environment, MB concentration = 5-40 mg·L-1).

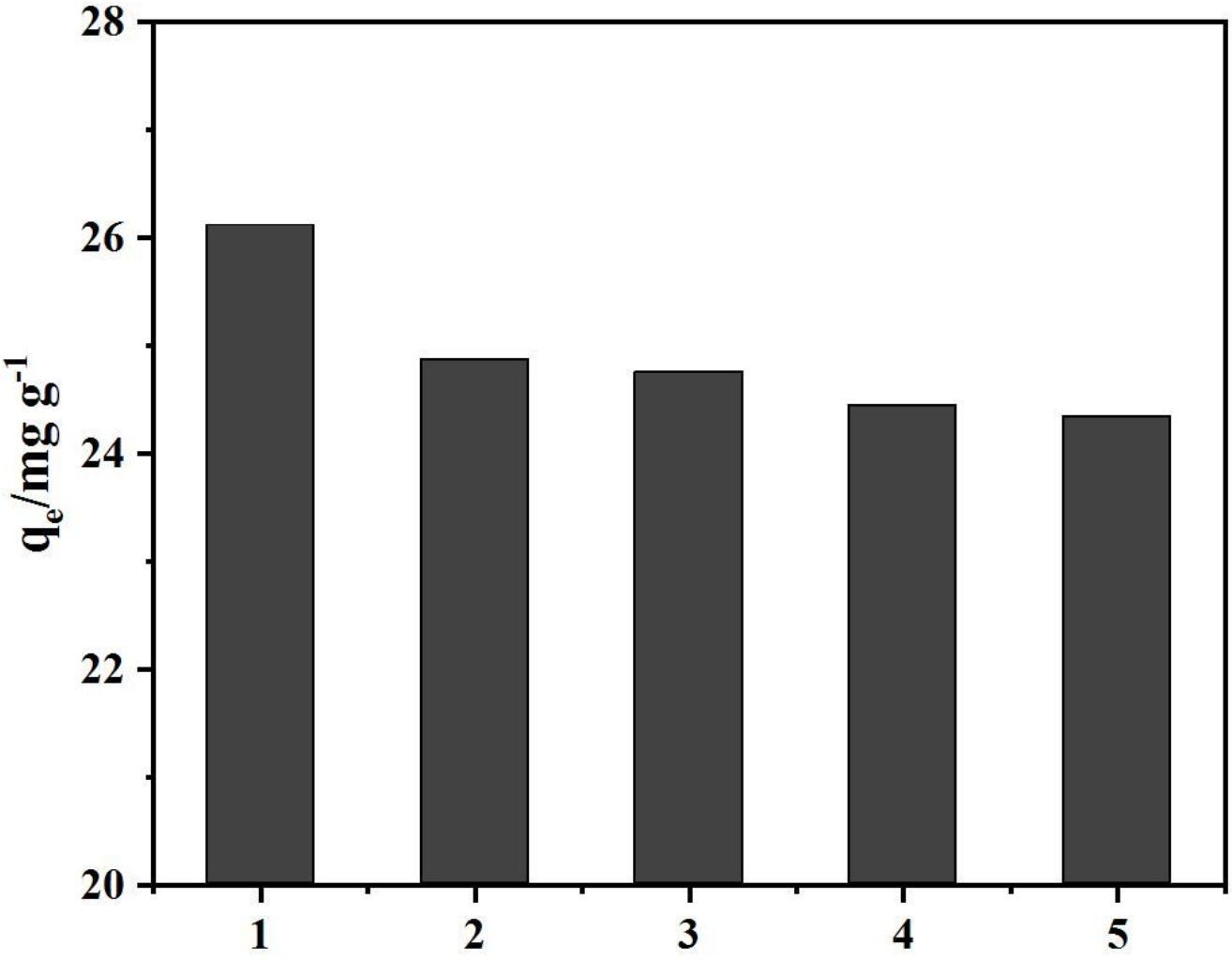

Figure 13

Effect of recycle time of QAS-β-CDPU-20% on adsorption efficiency.